PLOS | BIOLOGY

RESEARCH ARTICLE

Exosomes Mediate LTB_4 Release during Neutrophil Chemotaxis

Ritankar Majumdar, Aidin Tavakoli Tameh, Carole A. Parent*

Laboratory of Cellular and Molecular Biology, Center for Cancer Research, National Cancer Institute, National Institutes of Health, Bethesda, Maryland, United States of America

* parentc@mail.nih.gov

OPEN ACCESS

Citation: Majumdar R, Tavakoli Tameh A, Parent CA (2016) Exosomes Mediate LTB_4 Release during Neutrophil Chemotaxis. PLoS Biol 14(1): e1002336. doi:10.1371/journal.pbio.1002336

Academic Editor: Philippa Marrack, National Jewish Medical and Research Center/Howard Hughes Medical Institute, UNITED STATES

Received: June 29, 2015

Accepted: November 19, 2015

Published: January 7, 2016

Data Availability Statement: All relevant data are within the paper and its Supporting Information files.

Funding: This research was supported by the Intramural Research Program of the Center for Cancer Research, NCI, National Institutes of Health. The funders had no role in study design, data collection and analysis, decision to publish, or preparation of the manuscript.

Competing Interests: The authors have declared that no competing interests exists.

Abbreviations: AA, arachidonic acid; cAMP, cyclic adenosine monophosphate; CD63-GFP, GFP-tagged

Abstract

Leukotriene B_4 (LTB_4) is secreted by chemotactic neutrophils, forming a secondary gradient that amplifies the reach of primary chemoattractants. This strategy increases the recruitment range for neutrophils and is important during inflammation. Here, we show that LTB_4 and its synthesizing enzymes localize to intracellular multivesicular bodies that, upon stimulation, release their content as exosomes. Purified exosomes can activate resting neutrophils and elicit chemotactic activity in a LTB_4 receptor-dependent manner. Inhibition of exosome release leads to loss of directional motility with concomitant loss of LTB_4 release. Our findings establish that the exosomal pool of LTB_4 acts in an autocrine fashion to sensitize neutrophils towards the primary chemoattractant, and in a paracrine fashion to mediate the recruitment of neighboring neutrophils in trans. We envision that this mechanism is used by other signals to foster communication between cells in harsh extracellular environments.

Author Summary

Neutrophils represent the first line of attack against infections and inflammatory insults. The ability of neutrophils to reach these sites, a key feature in the resolution of infections, is mediated by their capacity to sense and migrate directionally to the core of the inflammation site. Chemicals released at the site of inflammation are known as primary attractants. The binding of these attractants to receptors on the surface of neutrophils leads to the secretion of secondary attractants that amplify the reach of primary attractants. We studied the mechanism by which secondary attractants are released from neutrophils. We found that the secretion of a key secondary attractant is mediated in the form of small vesicles called exosomes. These exosomes originate inside the cells, encapsulated in larger vesicles called multivesicular bodies. We purified exosomes from activated neutrophils and show that they contain the machinery to synthesize this secondary attractant and act specifically to elicit neutrophil motility. The inhibition of exosome release leads to a loss of secretion of the secondary attractant as well as a loss in directional motility. Together, our findings provide insight into the mechanisms cells use to protect labile attractants from

CD63; CI, chemotaxis index; CsH, cyclosporin H; DMSO, dimethylsulfoxide; EM, electron microscopy; ER, endoplasmic reticulum; EV, extracellular vesicle; FLAP, 5-LO activating protein; fMLP, N-formylMethionyl-Leucyl-Phenylalanine; GM-CSF, granulocyte macrophage colony-stimulating factor; ILV, intraluminal vesicles; KD, knockdown; LTA_4, leukotriene A_4; LTA_4H, leukotriene A_4 hydrolase; LTB_4, leukotriene B_4; LTB_4R1, receptor for LTB_4; mCherry-5LO, mCherry-tagged 5-LO; MLCII, myosin light chain II; MMP9, matrix metallopeptidase 9; MPO, myeloperoxidase; MVB, multivesicular body; NS, not significant; nSmase2, neutral sphingomyelinase 2; NSshRNA, nonspecific shRNA; 5-LO, 5-lipoxygenase.

harsh extracellular environments and communicate directional cues during inflammatory responses.

Introduction

Chemotaxis, the directed movement of cells in response to external chemical gradients, is essential to a wide array of biological processes ranging from developmental processes, wound healing, angiogenesis, and immune responses and is implicated in pathological conditions such as chronic inflammatory diseases and metastasis [1]. Upon exposure to endpoint primary chemoattractants, cells secrete secondary chemoattractants that serve to maintain the robustness and sensitivity to the primary chemoattractant signals [2]. Once secreted, these secondary chemoattractants form a gradient to recruit cells that are farther away, thereby dramatically increasing the range and persistence of detection [3]. Intercellular communication through the release of secondary chemoattractants may be homotypic, where the primary and secondary chemoattractant are the same, or it may be heterotypic, where the secondary chemoattractant is different from the primary chemoattractant and is released following stimulation by primary attractants. Homotypic intercellular communication is remarkably exhibited in the social amoebae *Dictyostelium discoideum*, where collective chemotaxis of cells towards cyclic adenosine monophosphate (cAMP) is regulated by the release of cAMP and the formation of characteristic chains of cells called streams [4]. Unlike cAMP in *Dictyostelium*, the release of the secondary chemoattractants CCL3 and CXCL8 by monocytes and dendritic cells in response to the primary chemoattractant Serum Amyloid A represents an example of heterotypic intercellular communication [5]. This ability of chemotaxing cells to transduce autocrine and paracrine chemical signals in response to primary signals has been termed signal relay.

Heterotypic signal relay occurs in neutrophils migrating towards primary chemoattractant gradients through the release of leukotriene B_4 (LTB_4) [6]. Following stimulation, cytoplasmic phospholipase $A_2\alpha$ translocates to the nuclear envelope, where it is poised to hydrolyze membrane bound lipids to form arachidonic acid (AA) [7]. Simultaneously, 5-lipoxygenase (5-LO) is mobilized to the nuclear envelope where it associates with the 5-LO activating protein (FLAP) and acts on AA to generate leukotriene A_4 (LTA_4). LTA_4, by means of LTA_4 hydrolase (LTA_4H), is finally converted into LTB_4 [7], which is then secreted from cells by an unknown mechanism. Initially thought to be released at the site of infection to mediate neutrophil recruitment and proinflammatory processes [8,9], LTB_4 was later shown to be a central secondary chemoattractant in vivo [10]. More recently, we showed that LTB_4 preferentially mediates neutrophil swarming towards tissue injury sites [11] and established that the secreted LTB_4 in physiological gradients of primary chemoattractants acts as an amplifier of neutrophil chemotaxis and mediates signal relay between migrating neutrophils [6].

In order for secondary chemoattractants to act as bona fide signal relay molecules, they must be released in a form that enables the generation of stable gradients during chemotaxis. It has been established that the release and subsequent diffusion of LTB_4 creates extremely transient gradients due to the small size of the molecule [12]. The self-diffusion coefficient of a typical formyl chemoattractant is ~ 10^{-5} cm^2/sec, which is a log order of magnitude higher than typical unsaturated fatty acids [13]. This implies extremely shallow LTB_4 concentration profiles. Indeed, assessment of the diffusive properties of AA, the structurally similar precursor of LTB_4, shows shallow and transient gradients compared to a primary chemoattractant such as N-formylMethionyl-Leucyl-Phenylalanine (fMLP) [12]. As a plausible mechanism to generate stable secondary gradients, one may argue in favor of a carrier-based mechanism for passive LTB_4 transport, such as binding

to serum albumin, and this may indeed be true for systemic transport [14]. This, however, would not account for short-range gradients in migrating cells owing to protracted and uncontrolled LTB_4 release. Moreover, this mechanism would not explain how hydrophobic molecules such as LTB_4 are protected from the aqueous environment of the extracellular milieu.

The mechanisms by which LTB_4 is secreted and how LTB_4 gradients are formed or mediate signal relay of primary chemotactic signals have yet to be determined. However, studies on gradient formation of lipid-modified *Drosophila* morphogens [15], or the formation of palmityolated-Wnt gradients during *Drosophila* embryogenesis [16] and cAMP gradient propagation in *Dictyostelium* [17], point towards vesicular packaging as an effective way of signal dissemination in the extracellular milieu. In the present study, we investigated whether a similar vesicular packaging of LTB_4 is involved in the creation of a stable gradient during neutrophil chemotaxis. To do so, we assessed whether LTB_4 is secreted though extracellular vesicles (EVs) and if its synthesis and transport involve intracellular vesicular trafficking. Most importantly, we also determined if vesicles released during chemotaxis are indeed capable of mediating the LTB_4-dependent signal relay response during neutrophil chemotaxis.

Results

5-LO Translocates to CD63 and LAMP1 Positive Fractions upon fMLP Addition

To begin identifying the mechanisms that underlie LTB_4 secretion, we measured LTB_4 content as well as the distribution of 5-LO in resting and activated neutrophils. We fractionated unstimulated and fMLP-stimulated primary human neutrophils using nitrogen cavitation, differential centrifugation, and separation on iodixanol density gradients (Fig 1A). In resting neutrophils, LTB_4 content was primarily low across the different fractions with a small peak observed in fraction 3 (Fig 1B). On the other hand, in fMLP-stimulated neutrophils, a nonuniform asymmetric increase of LTB_4 levels was observed, where LTB_4 levels were elevated in both low- (fractions 1–5; density ~1.05–1.08 g/ml) and high-density fractions (fractions 10–12; density ~1.17–1.19 g/ml), but not in intermediate density fractions (fraction 6–9; ~1.09–1.11 g/ml) that contained the cis-Golgi markers GM130 (Fig 1B and 1C). This fMLP-induced asymmetric partitioning of LTB_4 across different densities was unlike other canonical secretory proteins such as myeloperoxidase (MPO—a marker for the azurophilic granules) and matrix metallopeptidase 9 (MMP9—a marker for gelatinase granules) [18], although total MPO and MMP9 levels appeared to increase poststimulation (Fig 1C). These findings suggest that canonical secretory pathways used by MMP9 and MPO are not involved in LTB_4 trafficking. On the other hand, fMLP stimulation did induce the redistribution of the tetraspannin CD63 to higher density fractions. As CD63 is known to traffic between late endosomal and secretory compartments such as multivesicular bodies (MVBs) [19], we reasoned that CD63 redistributes to MVBs upon fMLP addition. This was confirmed by the presence of LAMP1, a high-density lysosomal marker shown to be present in MVBs of neutrophils [20], in fractions 9–12 (Fig 1C). Remarkably, 5-LO was also found in CD63- and LAMP1-positive high-density fractions upon fMLP stimulation, and the distribution pattern of LTB_4 was similar to that of 5-LO in both resting and activated conditions, suggesting active 5-LO in this cellular compartment. Together, the presence of LTB_4 and 5-LO in CD63- and LAMP1-positive fractions suggest the involvement of MVBs in LTB_4/5-LO transport.

5-LO Localizes on MVBs and Released Exosomes

To confirm whether the 5-LO-containing vesicles indeed reside in MVBs, we performed transmission electron microscopy (EM) on neutrophils chemotaxing towards fMLP. As previously

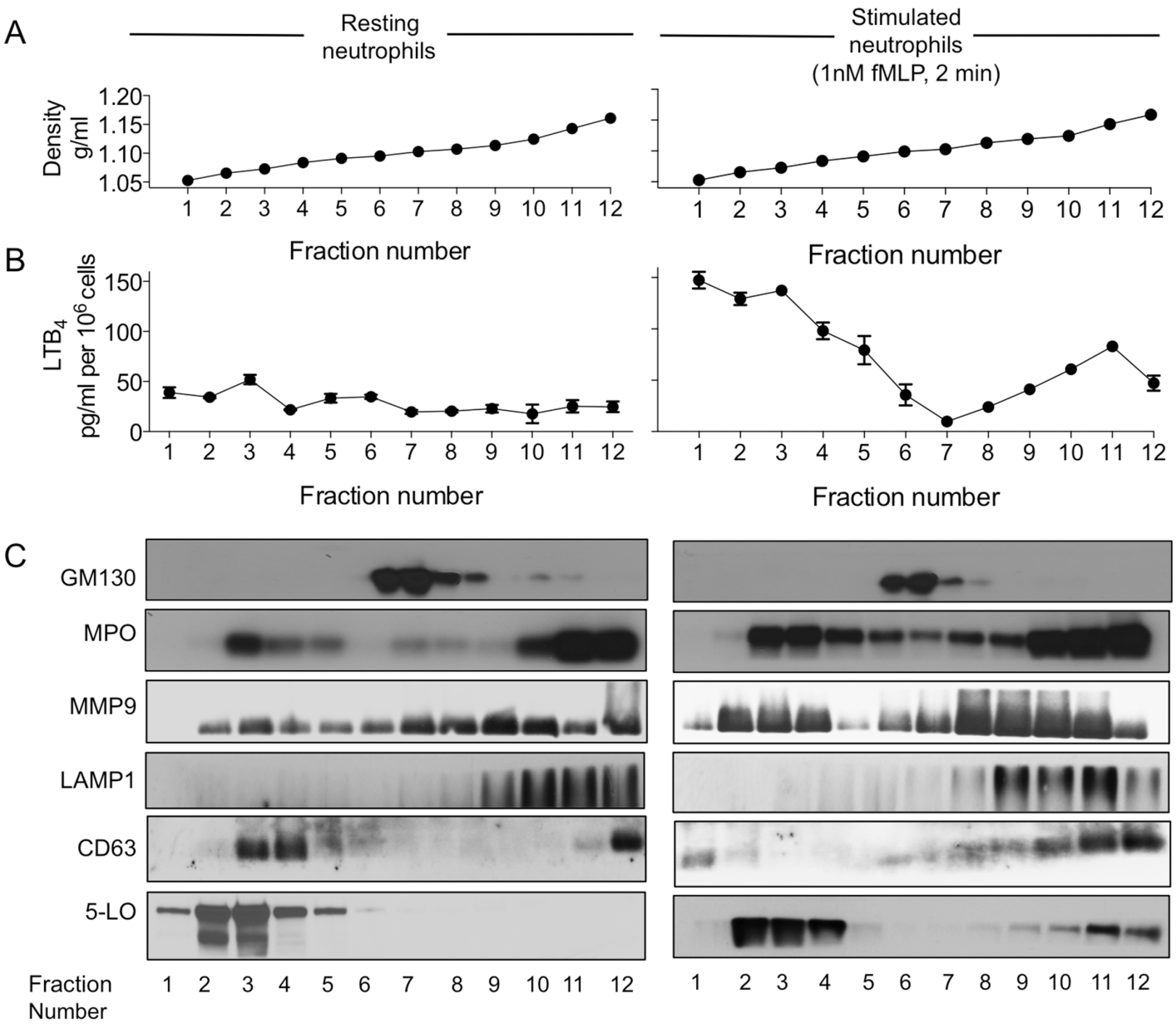

Fig 1. LTB_4 and 5-LO partition with CD63 and 5-LO positive fractions in continuous iodixanol gradients. (A) Mock-loaded continuous iodixanol gradients were fractionated, and the density of each fraction determined as described. **(B)** Nitrogen cavitates of freshly isolated primary human neutrophils were density fractionated on iodixanol gradients, and LTB_4 content from each fraction was extracted and measured by enzyme linked immunoassay (EIA). **(C)** Total protein from each fraction of iodixanol gradient described in panel B was precipitated using trichloroacetic acid, and western analysis was performed using specific antibodies. Data are representative of six independent experiments.

doi:10.1371/journal.pbio.1002336.g001

reported using immunofluorescence [21], we observed substantial 5-LO labeling on the nuclear envelope (Fig 2D, 2E and 2G) compared to antibody control (Fig 2A). Consistent with our fractionation findings, we also detected 5-LO on MVBs—both on the membrane and on intraluminal vesicles (ILVs) (Fig 2B–2E, 2G and 2I). Indeed, quantitation of immunogold staining of different vesicular compartments showed that the majority of 5-LO localized to MVBs compared to non-MVB vesicles (Fig 2F), with 30%–35% of all MVBs staining positive for 5-LO. In addition, 5-LO was observed on the plasma membrane (Fig 2B and 2C), which may be due to

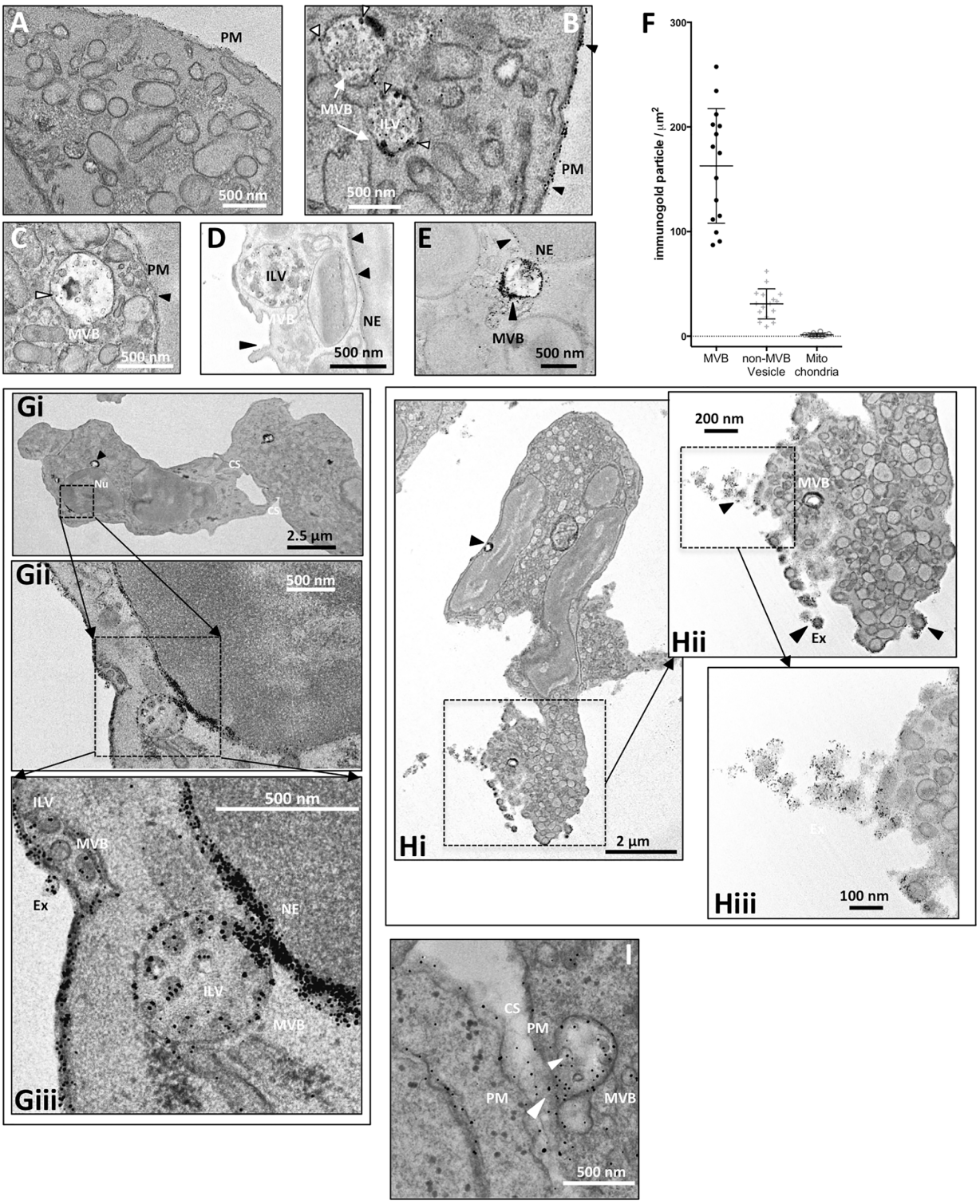

Fig 2. Ultrastructural analysis of the distribution of 5-LO in chemotaxing neutrophils. Representative immunogold EM images depicting the distribution of 5-LO in various cellular compartments in neutrophil chemotaxing towards fMLP. **(A)** Immunogold image stained with a normal rabbit IgG. **(B–E)** Immunogold images stained with a 5-LO-specific antibody. **(F)** Quantification of 5-LO positive staining in MVB, non-MVB vesicles, and mitochondria. **(G–H)** Progressive magnification of sections **(i through iii)** of neutrophils migrating towards fMLP showing formation and release of 5-LO-containing MVBs. **(I)** Fusion of 5-LO-containing MVB with plasma membrane and release of exosomes in cell synapse. Ne: nuclear envelope, Nu: nucleus, MVB: multivesicular body, ILV: intraluminal vesicles, Ex: exosome, PM: plasma membrane, CS: cell synapse.

doi:10.1371/journal.pbio.1002336.g002

the transfer of 5-LO-containing outer MVB membranes to the plasma membrane during fusion events (Fig 2Giii). Most interestingly, we found that a substantial number of 5-LO-containing MVBs (25%–30%) were tightly associated with the nuclear envelope (Fig 2E, 2G and 2Hi). These MVB-associated regions of the nuclear envelope also showed specific enrichment for 5-LO. MVBs typically fuse to the plasma membrane and release their ILVs, termed exosomes, into the extracellular milieu [22]. In this context, we readily observed 5-LO-containing ILVs released as exosomes from the trailing edge of neutrophils (Fig 2H) and the presence of 5-LO-containing vesicles at the synapse between two migrating neutrophils (Fig 2I).

As CD63 is highly enriched in exosomes [23], we next assessed the cellular distribution of 5-LO and CD63 in live chemotaxing cells. We expressed mCherry-tagged 5-LO (mCherry-5LO) and/or GFP-tagged CD63 (CD63-GFP) in the pluripotent hematopoietic cell line PLB-985, which can be differentiated into neutrophil-like cells [24]. We again found that 5-LO localizes to the nucleus in resting mCherry-5LO cells (S1A Fig and S1 Movie). However, upon uniform fMLP addition, we readily observed the redistribution of mCherry-5LO to the cytoplasm in a punctate pattern (Fig 3A and S2 Movie). This vesicular localization was even more apparent in cells chemotaxing in a gradient of fMLP and was found to be more prominent at the trailing edge compared to the leading edge of chemotaxing cells (Fig 3B and S3 Movie). The trailing edge localization of 5-LO-containing vesicles was further substantiated through phalloidin counterstaining, which marks the leading edge F-actin (S1B Fig). To determine the nature of the 5-LO positive vesicles, we visualized the dynamic distribution of CD63-GFP. As expected, we observed a punctate localization of the MVB marker in both resting (S1A Fig) and stimulated (S1C Fig) cells expressing CD63-GFP. Remarkably, in mCherry-5LO/CD63-GFP coexpressing cells chemotaxing towards fMLP, we observed a clear colocalization of both proteins (Fig 3C, S4 Movie), which again occurred mainly at the trailing edge of the chemotaxing cells. Together, these findings establish that 5-LO is present on MVBs that fuse with the plasma membrane and release their exosomal content during chemotaxis.

Neutrophils Release Exosomes Containing LTB_4 and LTB_4 Synthesizing Enzymes upon fMLP Addition

Having established the presence of 5-LO in MVBs, we set out to determine whether neutrophils secrete exosomes that contain LTB_4 and LTB_4 synthesizing enzymes. To this end, supernatants from fMLP-stimulated neutrophils were filtered through 0.45 μm pore-sized membranes and centrifuged to remove larger vesicles and cell fragments. Pellets recovered from ultracentrifugation of the filtrate contained a heterogeneous mixture of EVs (unpurified EV) ranging in size from 50–500 nm, as ascertained from by EM (Fig 3D). Crude EVs were further fractionated on a discontinuous gradient of iodixanol to yield a vesicle population with a density of ~1.09 g/ml and vesicle size between 50–120 nm (median vesicle size = 80 nm; Fig 3D)—a characteristic size for exosomes [25]. We found that the purified vesicles were enriched in the tetraspannins CD63 and CD81, also reported in exosomes [23], and had very low amounts of the endoplasmic reticulum (ER) integral protein Calnexin or the ER lumen marker GRP94 (Fig 3E). Furthermore, the possibility of contamination from ectosomes and other plasma membrane-derived vesicles was excluded by the absence of the ectosome marker CD11b in purified vesicles (S2A Fig) [26]. We also found that the release of exosomes from neutrophils increased upon fMLP addition, as the detection of the exosomal markers CD63 and CD81 increased with fMLP treatment (Fig 3F). This increase was dependent on the concentration of fMLP added to cells (S2B Fig). Moreover, the release of exosomes from cells was also observed following ionomycin addition but not with granulocyte macrophage colony-stimulating factor (GM-CSF) treatment (S2C Fig). Most importantly, we determined that the enzymes responsible for the

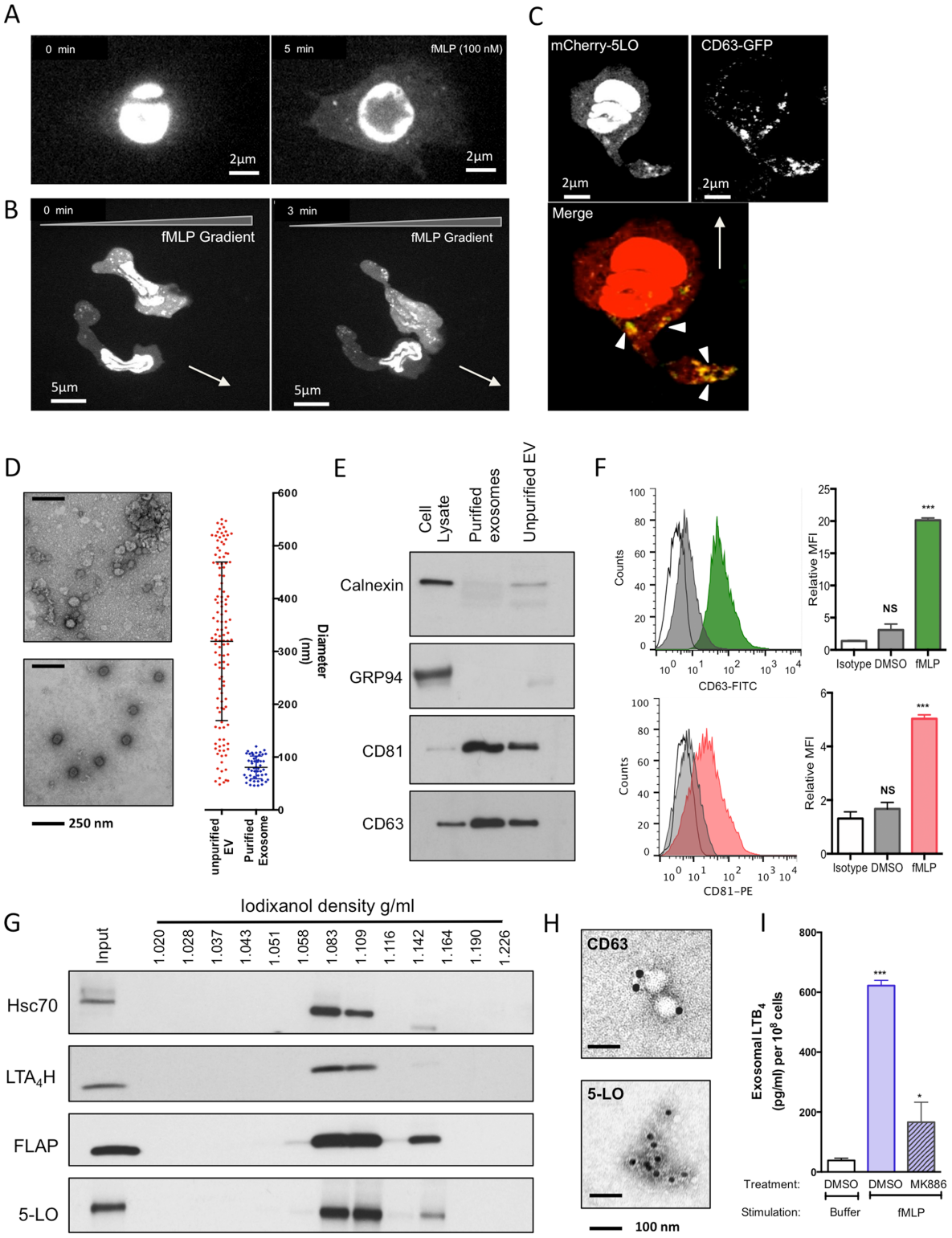

Fig 3. Neutrophils release exosomes containing LTB_4 and LTB_4-synthesizing enzymes upon fMLP addition. (A) Differentiated mCherry-5LO cells were plated on fibronectin-coated plates, and time-lapse images were captured before and after a uniform stimulation with 10 nM fMLP. Fluorescent images are representative of six independent experiments. Also see S1 and S2 Movies. **(B)** Differentiated mCherry-5LO cells were allowed to chemotax under agarose towards an fMLP gradient. Time-lapse images were captured 30 min after the addition of fMLP, 700 µm away from the chemoattractant well. Gradient slope ~ 50 pM/µm (see Materials and Methods). Fluorescent images are representative of 20 independent experiments. Also see S3 Movie. **(C)**

Differentiated CD63-GFP/mCherry-5LO coexpressing cells were allowed to chemotax as described in B. Fluorescent images are representative of eight independent experiments. Also see S1 Fig and S4 Movie. **(D)** Negatively stained EM images of pellets obtained from filtration and ultracentrifugation of supernatants of fMLP-stimulated neutrophils (upper panel) and after further purification on a discontinuous iodixanol gradient (lower panel). Vesicle sizes were determined from five vesicles from five fields from three independent experiments. **(E)** Equal amounts of protein from purified exosomes, crude ultracentrifugation pellets, and total cell lysates (10 μg) were subjected to western analysis using Calnexin, GRP94, CD81, and CD63 specific antibodies. Results are representative of three independent experiments. **(F)** Detection of CD63 (upper panel) or CD81 (lower panel) on exosomes obtained from fMLP-stimulated or dimethyl sulfoxide (DMSO)-treated neutrophils in a bead-based flow cytometry assay. Relative median fluorescence intensities obtained from three independent experiments are shown as mean ± standard deviation (SD). *** and NS (Not Significant) indicate $p < 0.0001$ and $p > 0.05$, respectively, compared to the isotype control. Also see S2 Fig. **(G)** Crude ultracentrifugation pellets were loaded on a discontinuous iodixanol gradient, total protein from each fraction precipitated and subjected to western analysis using antibodies for the exosomal marker HSC70 or LTB_4 synthesizing enzymes. 5% of the total input was analyzed. Results are representative of three independent experiments. **(H)** Representative immunogold EM images of exosomes from stimulated neutrophils stained with CD63 or 5-LO antibodies. **(I)** Purified exosomes from fMLP-stimulated neutrophils treated with DMSO or MK886 (1 μM, 30 min) were lysed and their LTB_4 content measured using EIA. Results from four independent experiments are shown as mean ± SD. *** and NS indicate $p < 0.0001$ and $p > 0.05$, respectively, compared to the LTB_4 content of exosomes purified from vehicle treated nonstimulated cells.

doi:10.1371/journal.pbio.1002336.g003

synthesis of LTB_4, namely 5-LO, FLAP, and LTA_4H, were all present in fractions containing HSC70 (another known exosome marker [27]) (Fig 3G) and EM analyses revealed that both 5-LO and CD63 specifically decorate exosomes isolated in these fractions (Fig 3H). The exosomes isolated from fMLP-stimulated neutrophils showed a high LTB_4 content, which was dramatically reduced by pretreating neutrophils with the FLAP inhibitor MK886 (Fig 3I). Together, these findings show that upon fMLP addition, neutrophils release exosomes containing LTB_4 and the enzymes required for its synthesis.

Exosomes Activate Neutrophils in an LTB_4-Dependent Manner

We next studied the extent by which exosomes mediate the effects of LTB_4 on neutrophil function. We first purified exosomes from mCherry-5LO and CD63-GFP expressing cells following fMLP treatment in the presence and absence of MK886 and measured their LTB_4 content. We found that the exogenous expression of either mCherry-5LO or CD63-GFP significantly increases exosomal LTB_4 (Fig 4A) and, as we observed with neutrophils (Fig 3I), LTB_4 content was dramatically inhibited by pretreatment with MK886 (Fig 4A). Quantification of the released exosomes showed that the decrease in LTB_4 content in MK886-treated cells was not a result of a decrease in exosome release by these cells (Fig 4B). More importantly, the addition of exosomes derived from mCherry-5LO or CD63-GFP expressing cells to neutrophils rapidly induced cellular polarization and adhesion, indicating that the exosomes readily activate resting neutrophils (Fig 4C). These observations were further strengthened by the increase of both pErk1/2 and pAkt levels upon the exogenous addition of exosomes from mCherry-5LO or mCherry expressing cells to resting neutrophils (Fig 4D and S3A Fig). Of note, the extent by which the exosome preparations increased pErk1/2 and pAkt levels was greater in cells exposed to mCherry-5LO exosomes versus mCherry exosomes (S3A Fig), which could reflect the higher LTB_4 content of exosomes derived from mCherry-5LO expressing cells, compared to mCherry expressing cells (Fig 4A).

The EZ-Taxiscan microfluidic device was used to assess whether exosomes are capable of inducing a chemotactic response. As seen in Fig 4E and S5 Movie, neutrophils were able to migrate towards exosomes derived from mCherry-5LO expressing cells with speeds and chemotactic indices (CIs) comparable to those observed in the presence of LTB_4 alone. To determine whether the chemotactic response was mediated by LTB_4, we exposed neutrophils treated with the LTB_4 receptor-1 antagonist LY223982 to exosomes. We found that LY223982 treatment dramatically reduced the chemotactic response of neutrophils to both LTB_4 and exosomes derived from mCherry-5LO-expressing cells (Fig 4F and S6 Movie). The antagonist-treated cells, however, did not show migration defects to saturating concentrations of fMLP, showing that LY223982 treatment did not impede chemotaxis due to nonspecific effects (S3B

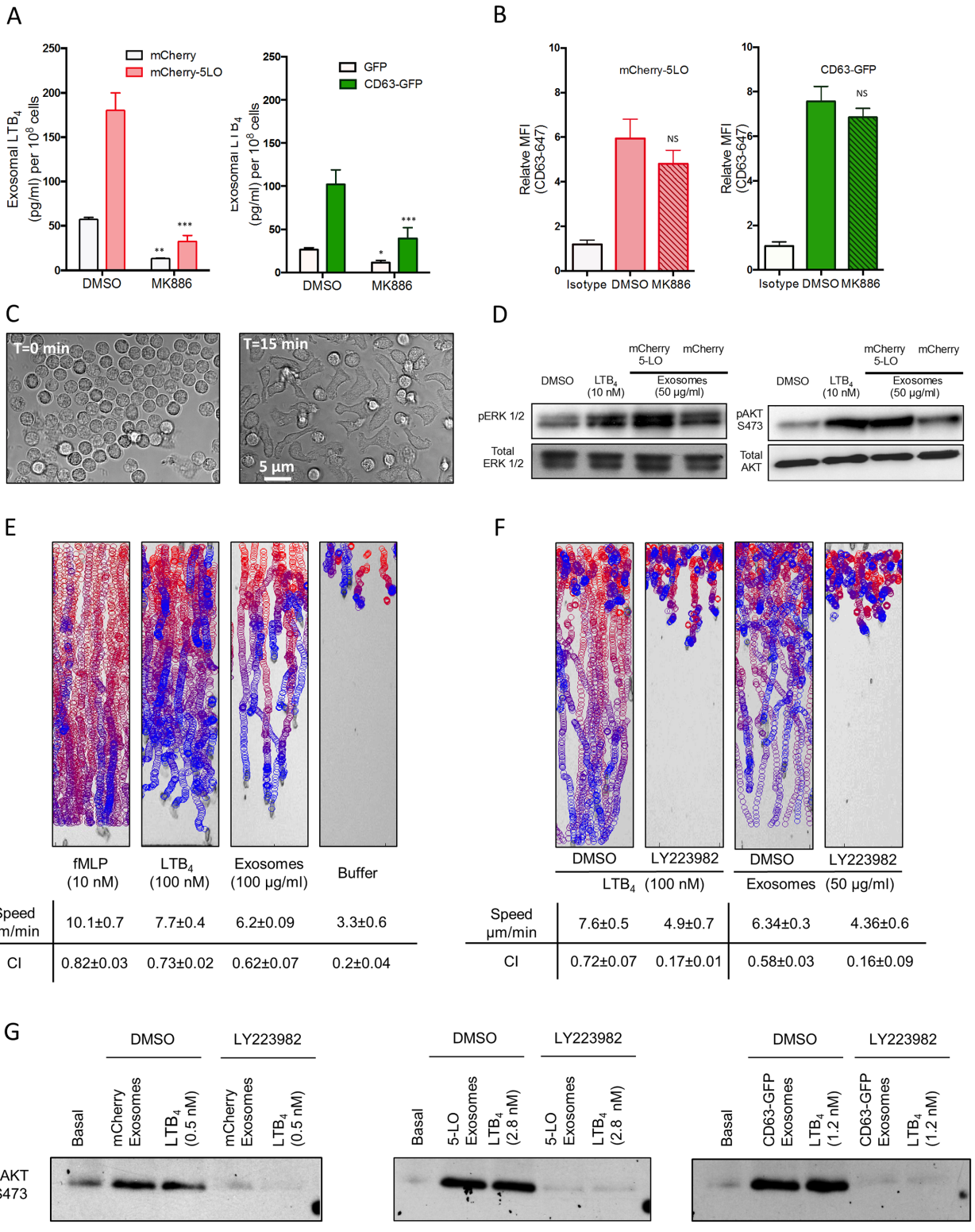

Fig 4. Exosomes activate neutrophils in an LTB_4-dependent manner. (A) Exosomes were purified from differentiated mCherry-5LO or CD63-GFP cells pretreated with either DMSO or MK886 (1 μM, 30 min) and subsequently stimulated with 2 nM fMLP. The exosomes were lysed and their LTB_4 content measured by EIA. Results from four independent experiments are shown as mean ± SD. The symbols ***, **, *, and NS indicate $p < 0.0001$, $p < 0.001$, $p < 0.01$, and $p > 0.05$, respectively, compared to corresponding DMSO-treated controls. **(B)** Detection of CD63 on exosomes purified from differentiated mCherry-5LO or CD63-GFP cells that were pretreated with either DMSO or MK886 (1 μM, 30 min) and subsequently stimulated with 2 nM fMLP in a bead-

based flow cytometry assay. Relative median fluorescence intensities obtained from four independent experiments are shown as mean ± SD. NS indicates statistical insignificance ($p > 0.05$) of the number of exosomes derived from MK886-treated cells compared to DMSO controls. **(C)** Neutrophil adhesion to fibronectin-coated plates was observed before and 15 min after the addition of 10 μg exosomes derived from mCherry-5LO cells. Differential interference contrast images are representative of three independent experiments. **(D)** LTB_4 (10 nM) or exosomes (50 μg/ml) isolated from mCherry or mCherry-5LO cells was added to the neutrophils for 15 min and pAkt S473 and p44/42 MAPK (Erk1/2) (T202/Y204) were determined by western analysis using specific antibodies. Data are representative of four independent experiments. See S3A Fig for quantitation. **(E)** EZ-Taxiscan chemotaxis towards fMLP, LTB_4, exosomes derived from mCherry-5LO expressing cells, or control buffer. The images show paths of individual cells migrating as circles (from red to blue with increasing time) overlaid onto the final frame. Corresponding migration speeds and chemotaxis index (CI) were calculated from three different experiments and represented as mean ± SD. Also see S5 Movie. **(F)** Neutrophils were treated with DMSO or LY223982 (10 μM for 30 min) and allowed to migrate towards LTB_4 or exosomes derived from mCherry-5LO expressing cells. Corresponding migration speeds and CI are calculated from 3 different experiments and represented as mean ± SD. Also see S3B Fig and S6 and S7 Movies. **(G)** Exosomes derived from mCherry, mCherry-5LO, or CD63-GFP expressing cells were divided into two parts. One part was used to measure LTB_4 levels to be added exogenously to neutrophils (control or LY223982 treated). The other part was added to neutrophils and pAkt (S473) levels were assessed after 15 min incubation. Data are representative of three independent experiments. See S3C Fig for quantification.

doi:10.1371/journal.pbio.1002336.g004

Fig). We also observed that exosomes derived from MK886-treated mCherry-5LO cells displayed weak chemotactic activity compared to exosomes from control treated cells (S7 Movie), further showing that the LTB_4 present in exosomes is responsible for the chemotactic behavior. These results were confirmed biochemically by assessing the effects of the exogenous addition of LTB_4 or exosomes on pAkt in neutrophils pretreated with LY223982. As shown in Fig 4G, LTB_4 or exosome addition gave rise to equal levels of pAkt for each exosome preparation and LTB_4 amounts used and, most importantly, the pAkt response was blocked by pretreating the cells with LY223982 (see S3C Fig, for quantification). Together, these findings establish the central role of LTB_4 in exosome-mediated neutrophil activation.

Reduced Exosome Production Leads to a Decrease in Exosomal LTB_4 Release and a Loss in Directional Migration

To specifically assess the role of exosome formation and release for LTB_4 secretion, we knocked down Rab27a or neutral sphingomyelinase 2 (nSmase2; SMPD2 gene) using small hairpin RNAs (shRNA) in PLB-985 cells. Rab27a is critical in MVB docking to the plasma membrane, and its depletion was shown to reduce exosome secretion [28,29]. nSmase2 is important in exosome secretion by mediating the budding of exosomes into MVBs [30]. We achieved an efficient knockdown (KD) of Rab27a and SMPD2 expression in both undifferentiated and differentiated PLB-985, and the KD of one gene did not alter the expression of the other (S4A Fig). Of the six shRNA sequences screened for each gene, we selected Rab27a shRNA 1 (sh1) and Rab27a shRNA 3 (sh3) for further studies (presenting 75% ± 4% and 70% ± 8% reduction of protein levels, respectively), whereas shRNA 2 (sh2) and shRNA 4 (sh4) were selected for SMPD2 (presenting 82% ± 8% and 85% ± 6% reduction in protein levels, respectively). Using CD63 and CD81 as markers, we found that both SMPD2 and Rab27a KD cells show reduced exosome production upon treatment with 2 nM fMLP compared to control nonspecific shRNA (NSshRNA) cells (Fig 5A and S4B Fig). The purity of the exosome preparations was assessed using the ectosome marker CD11b. Similarly, LTB_4 content of purified exosomes from both KD cell lines was markedly lower than in control cell lines (Fig 5B), although LTB_4 levels across the different cell types were not different when normalized to the total exosomal protein content (Fig 5C). These findings indicate that depletion of either nSmase2 or Rab27a does not affect LTB_4 synthesis. When we measured the total amount of LTB_4 secreted from each cell line in response to 1 nM fMLP, a physiological relevant concentration, we also observed a 75%–85% reduction in KD cells compared to control (Fig 5D). Interestingly, stimulating cells with a saturating concentration of fMLP (1 μM) reduced total LTB_4 secretion by 40%–50%. Although this could result from residual Rab27a or nSmase2 activity in the KD cell lines, nonexosomal sources of LTB_4 could become dominant under bulk activation conditions.

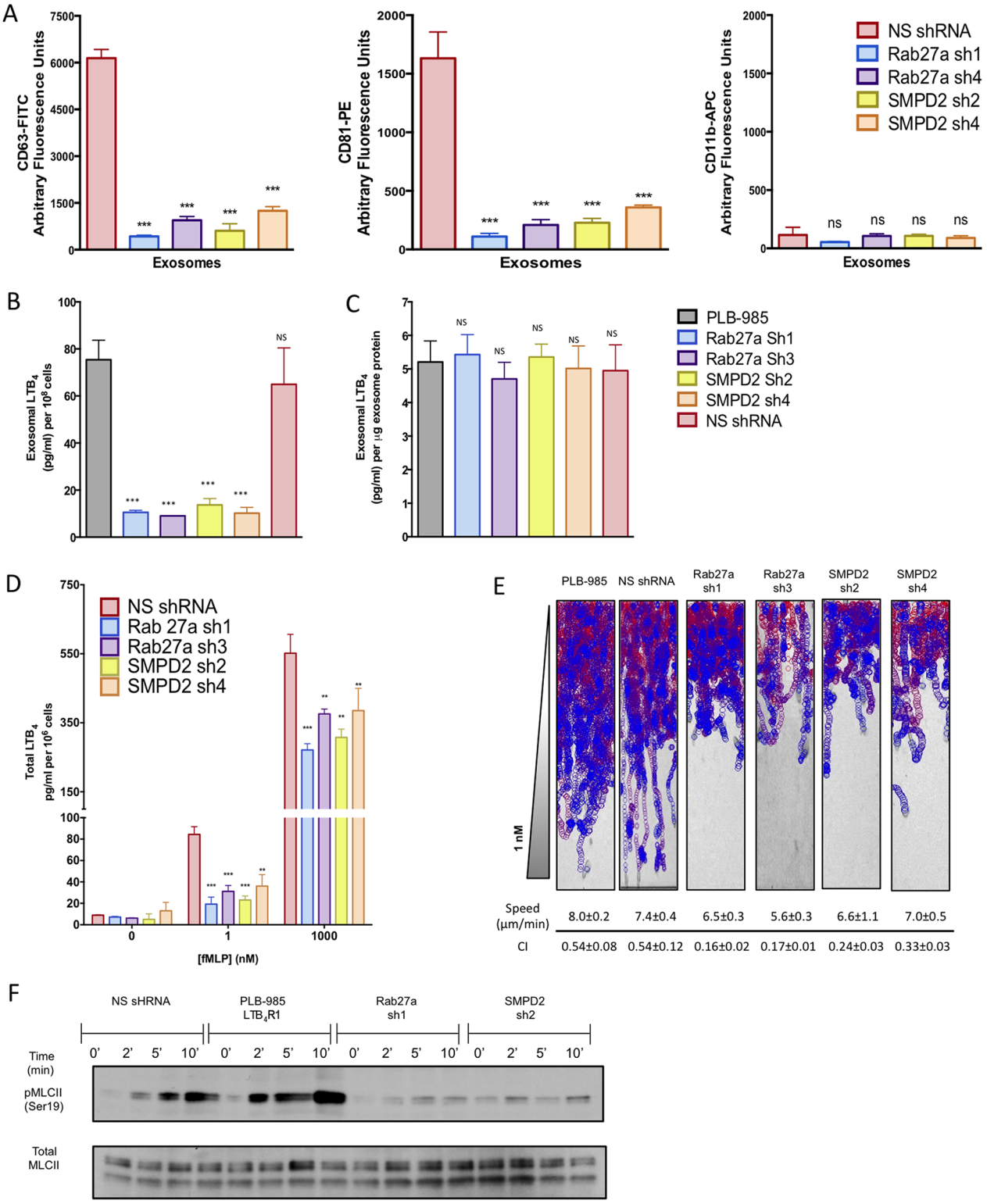

Fig 5. Rab27a and SMPD2 KD cells release less exosomes and show a loss in directional migration. (A) Exosomes were purified from differentiated control (NS shRNA), Rab27a shRNA (sh1; sh3), or SMPD2 shRNA (sh2; sh4) KD cells after treatment with fMLP (2 nM, 30 min) and analyzed using a bead-based flow cytometry assay with CD63-FITC, CD81-PE, and CD11b-APC conjugated antibodies. Panels show quantitative analysis from three independent experiments as mean ± SD. Evaluation of exosome flow cytometry was done as described in the legend of S2A Fig. See S4B Fig, for flow cytometry graphs. **(B–C)** Exosomes were purified from differentiated control and shRNA KD cells stimulated with 2 nM fMLP. The exosomes were lysed and their LTB$_4$ content

measured by EIA. Results from four independent experiments are shown as mean ± SD in pg/ml/10^8 cells (**B**) or pg/ml/μg of exosome protein (**C**). *** and NS indicate $p < 0.0001$ and $p > 0.05$, respectively, compared to corresponding control PLB-985 cells. **(D)** Differentiated control and shRNA KD cells were stimulated with subsaturating (1 nM) or saturating (1 μM) fMLP for 10 min, and the amount of LTB_4 in the supernatant was assessed by EIA. Results from three independent experiments are shown as mean ± SD. The symbols ** and *** indicate $p < 0.001$ and $p < 0.0001$, respectively, compared to corresponding NS shRNA controls. (**E)** EZ-Taxiscan chemotaxis towards 1 nM of control and KD cell lines. Corresponding migration speeds and CI were calculated from four different experiments and represented as mean ± SD. See legend of Fig 4E for details. Also see S8 Movie. (**F)** Differentiated NSshRNA, Rab27a, or SMPD2 KD cells or PLB-985 cells overexpressing LTB_4R1 were plated on fibronectin-coated plates for 10 min and uniformly stimulated uniformly with 1 nM fMLP. At specific time points, samples were subjected to western analyses using an antibody against phospho and total myosin light chain II (MLCII). Data are representative of three independent experiments. See S5C Fig, for quantification.

doi:10.1371/journal.pbio.1002336.g005

We next set out to assess the chemotactic behavior of the KD cell lines. We found that KD of either SMPD2 or Rab27a specifically reduced the directional motility (or CI) of cells towards a subsaturating concentration of fMLP (effective concentration 1 nM) (Fig 5E and S8 Movie), as the speed of migration remained unchanged for both KD cell lines (Fig 5E). To further investigate whether exosomes play a role in the relay of primary chemotactic signals, we measured myosin light chain II (MLCII) phosphorylation following a subsaturating fMLP stimulation, a process acutely affected by the disruption of LTB_4 signaling in neutrophils [6]. As we previously reported, we measured an increase in pMLCII levels in cells expressing NSshRNA in response to 2 nM fMLP (Fig 5F). We also found that the increase of pMLCII levels was further accentuated in PLB-985 cells over expressing the receptor for LTB_4 (LTB_4R1), suggesting higher sensitivity of LTB_4R1 expressing cells towards signal relay processes and the pivotal role that LTB_4 plays in this response (Fig 5F). In sharp contrast, and as observed in neutrophils where LTB_4 synthesis is inhibited [6], no fMLP-mediated pMLCII increase was measured in either Rab27a or SMPD2 KD cells (Fig 5F and S4C Fig). Together, these findings show that exosome release regulates LTB_4 secretion and signal relay during neutrophil chemotaxis.

Importantly, the defects of the KD cells appeared to be highly specific. Both SMPD2 and Rab27a KD cells did not show defects in their ability to adhere upon fMLP stimulation (S5A Fig), nor did they show any defect in their ability to increase pERK1/2 upon fMLP stimulation (S5B Fig). Furthermore, as we found with MK8886 treatment [6], the defects in directional migration were absent when a saturating concentration of fMLP (effective concentration 100 nM) was used (S5C Fig and S9 Movie). Together, these findings indicate that neither Rab27a nor nSmase2 regulate the ability of cells to respond to fMLP and rule out KD specific bystander effects.

Exosomal LTB_4 Acts in an Autocrine and Paracrine Fashion during Neutrophil Chemotaxis

We next sought to determine whether exosomal LTB_4 acts in an autocrine and/or paracrine fashion during neutrophil chemotaxis. To do so, we labeled neutrophils with cytotracker red and tracked their movement as they chemotaxed towards fMLP using the under agarose assay. To quantify the data, we color-coded the displacement tracks as a function of the imaging time; blue representing the cell's position during initial periods of migration and red the final. We found that compared to control cells (Fig 6Ai; S10 Movie), MK886-treated cells migrated shorter distances and with less direction, although speed of migration was not affected (Fig 6Aii; S10 Movie). We also found that treatment with GW4869, an nSmase2 inhibitor, and a known inhibitor of exosome production [30] (S6A Fig), similarly affected chemotactic motion (Fig 6Bi and 6Bii; S11 Movie). Furthermore, and consistent with the chemotaxis defect of SMPD2 KD cells using the EZ-Taxiscan system (Fig 5E), we observed a similar loss in CI and distance migrated in SMPD2 shRNA KD cells (S6B Fig). We then asked if these defects could be rescued by the paracrine action of an exogenous source of exosomes. For this purpose, we

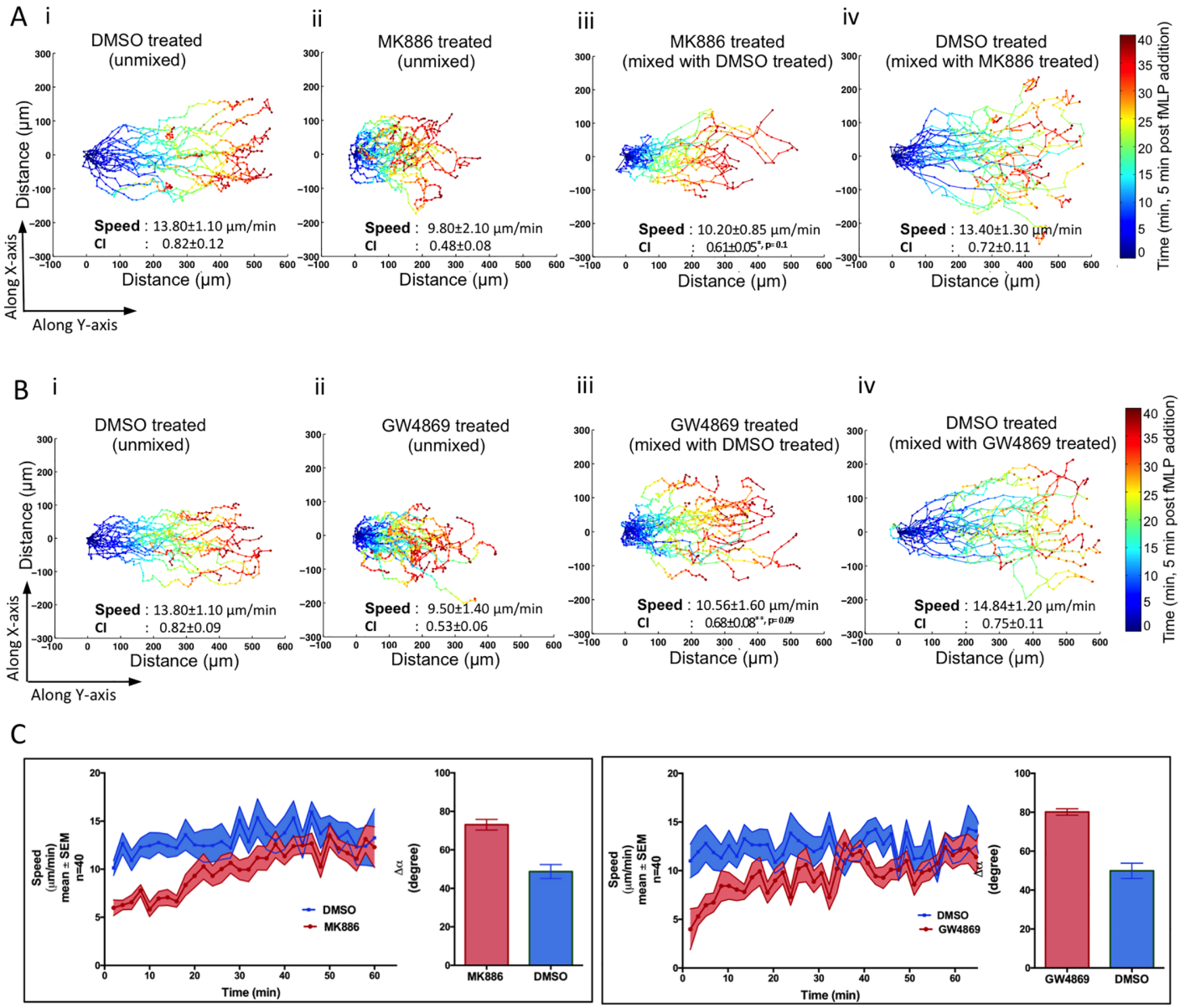

Fig 6. Exosomes mediate the paracrine and autocrine effects of LTB_4. (A) Cell tracks of neutrophils chemotaxing towards a ~50 pM/μm gradient of fMLP under agarose (see Materials and Methods). **(i)** DMSO-treated cells stained with cytotracker red. **(ii)** MK886-treated cells stained with cytotracker red. **(iii–iv)** MK886-treated cells stained with cytotracker red mixed with DMSO-treated cells stained with cytotracker green: **(iii)** shows the tracks of MK886-treated red cells in the mixture and **(iv)** shows tracks of DMSO-treated green cells in the mixture. Speed and CI were calculated from the tracks of 40 cells and averaging over six independent movies. The temporal location of cells in the X or Y direction is coded according to the color map shown. Also see S10 Movie. **(B)** Cell tracks of neutrophils chemotaxing towards fMLP as described in legends of A. In this case, neutrophils were treated with GW4869. Red cells were tracked in panels i, ii, and iii. In panel iv, DMSO-treated cells stained with cytotracker green were tracked. Speed and CI were calculated from the tracks of 40 cells and averaging over six independent movies. Also see S6B Fig and S11 Movie. **(C)** Graphs depicting the change in the speed of control- (labeled blue) or inhibitor- (labeled red) treated cells as a function of time. The mean average change in the angular deviation (Δα) between two consequent tracks is presented in the bar graph. Data were calculated from the tracks of 40 cells and averaging over six independent movies. *** indicates $p < 0.0001$ compared to DMSO treated cells.

doi:10.1371/journal.pbio.1002336.g006

mixed untreated neutrophils (labeled green) and treated (MK886 or GW4869) neutrophils (labeled red) in equal proportion and recorded their motility towards fMLP. We observed a dramatic improvement of both directionality and total distance migrated in MK886- (Fig 6Aiii; S10 Movie) and GW4869-treated neutrophils (Fig 6Biii; S11 Movie). No difference was found

in the motility of untreated cells labeled either with the green or red dyes (Fig 6Ai & 6Aiv and 6Bi & 6Biv), excluding any dye-specific effects. Furthermore, NSshRNA cells similarly rescued the directionality defect of SMPD2 shRNA KD cells (S6B Fig).

While we observed a dramatic improvement in the CI of GW4869- or MK886-treated cells through the paracrine effects of exosomal LTB_4 (Fig 6A and 6B), we noticed that the treated cells showed defects in the time required to migrate towards fMLP (Fig 6C). It required up to 35 min for cells treated with either drug to traverse 300 μm, compared with 20 min for untreated cells (Fig 6A and 6B). In addition, the treated cells exhibited slower speeds as well as a loss of directional persistence in the initial phases of migration (Fig 6C). These defects in migration initiation and sensitization to a chemoattractant cue highlight a key role for exosomal LTB_4 in autocrine signaling.

One may argue that exosomal LTB_4 merely increases the robustness of the chemotactic response by regulating the cellular machinery as opposed to acting as a chemotactic beacon. We tested this by mixing cells that cannot detect fMLP with cells defective in exosome release and observed their migration towards fMLP. Due to their higher sensitivity to LTB_4, we used LTB_4R1 overexpressing cells as receiving cells in these experiments (Fig 5F). We treated green-labeled LTB_4R1 cells with the FPR-1 antagonist cyclosporin H (CsH) [31] and mixed them with red-labeled cells expressing control shRNA (NSshRNA), which were also treated with CsH. These cells did not migrate towards fMLP, confirming the efficacy of the antagonist treatment, and no such defects were observed when control-labeled cells were mixed (Fig 7A). However, the motility defect of CsH-treated LTB_4R1 cells was readily rescued when mixed with untreated NSshRNA cells, but not with MK886-treated NSshRNA cells (Fig 7B). These findings reiterate that LTB_4 released by NSshRNA cells is responsible for the trans-recruitment of CsH-treated cells. Importantly, no rescue in motility was observed in CsH-treated LTB_4R1 cells when they were mixed with Rab27a or SMPD2 KD cells (Fig 7C) and in GW4869- or MK866-treated neutrophils (S7 Fig). Together, these observations indicate that exosomal LTB_4 relays chemotactic signals in response to primary attractants during neutrophil chemotaxis.

Discussion

Our prior studies on neutrophils migrating in chemotactic gradients identified LTB_4 as an important signal relay molecule that increases the recruitment range of neutrophils to sites of inflammation [6,11]. This observation led us to study the mode of LTB_4 release from cells and its effective dissemination. In this study, we show that LTB_4 is packaged in MVBs that are released as exosomes during neutrophil chemotaxis. We present this as a mechanism through which hydrophobic low-diffusible lipid molecules, like LTB_4, mediate the signal relay process. Our study proposes that neutrophils migrating in primary chemoattractant gradients release exosomes containing LTB_4 and LTB_4 synthesizing enzymes. These exosomes subsequently act in an autocrine manner—by sensitizing cells towards the primary chemoattractant—and in a paracrine manner, by acting as molecular beacons for following cells (Fig 8).

We found that both LTB_4 and 5-LO are present in MVBs and exosomes, which also contain LTA_4H and FLAP. The presence of LTB_4 synthesizing enzymes has previously been reported in exosomes derived from macrophages and dendritic cells [32]. However, unlike dendritic cells that constitutively produce exosomes [33], we detected little or no release of exosomes in unstimulated neutrophils. Instead, we observed exosome release upon treatment with ionomycin as well as following the addition of fMLP, but not GM-CSF, indicating that exosome release is a result of primary stimulation and not a priming event. fMLP is also known to increase the release of plasma membrane-derived secretory vesicles and ectosomes [34] that have considerable overlap with exosomes in terms of size (50–200 nm). However, owing to their differences

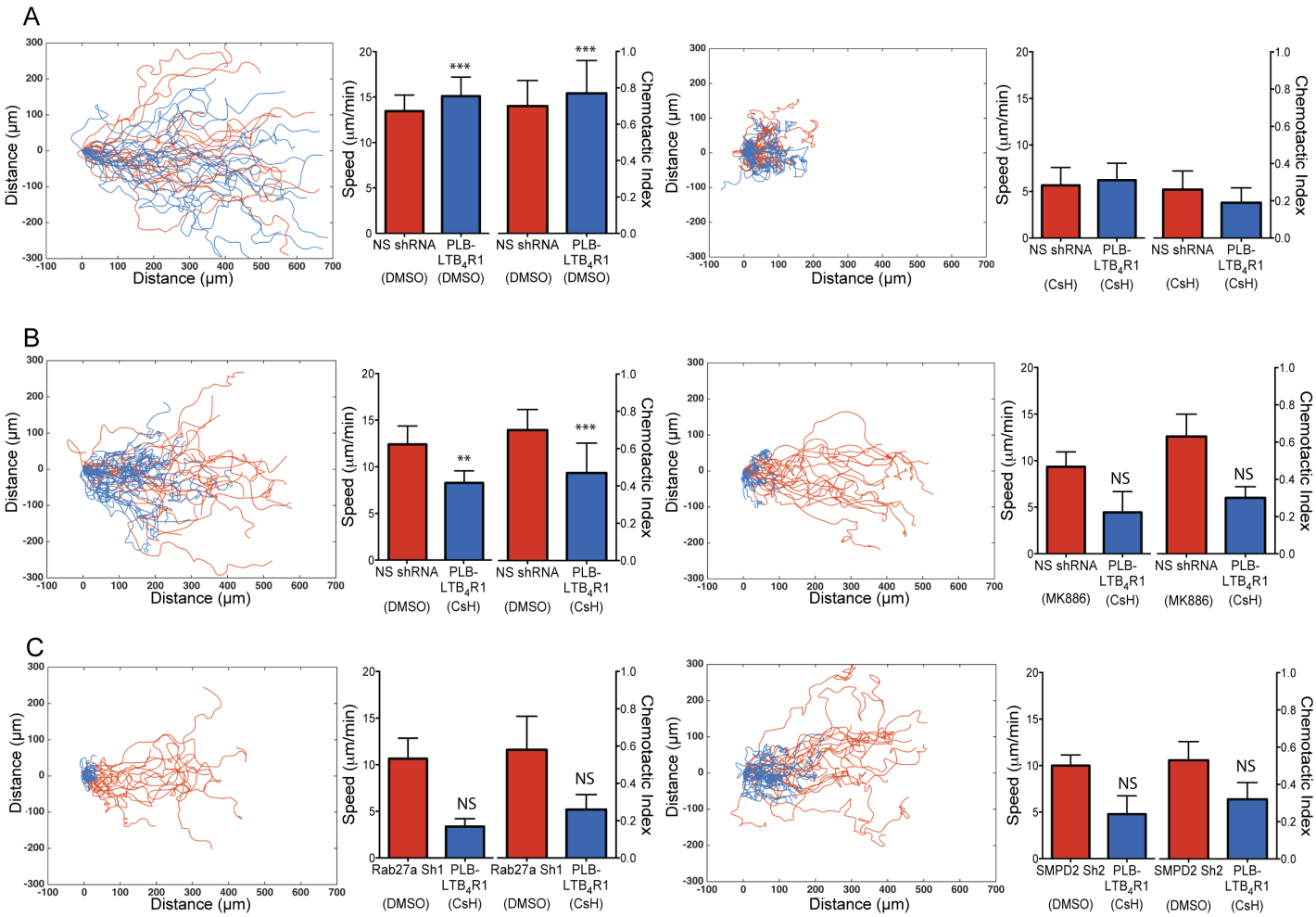

Fig 7. Exosomes mediate signal relay during neutrophil chemotaxis. Tracks, speed, and CI of mixtures of cytotracker-labeled cell lines migrating under-agarose towards a ~50 pM/μm gradient of fMLP. Also see S7 Fig and S12 Movie. **(A)** Differentiated cells overexpressing the LTB$_4$R1 (labeled with cytotracker green, shown as blue tracks) in a mixture with NS shRNA cells (labeled with cytotracker red, shown as red tracks) treated with DMSO (left) or CsH (right). Composite graph shows displacement tracks of both types of cells. Speed and CI were calculated from the tracks of 40 cells and averaging over 8 independent movies. **(B)** Differentiated cells overexpressing the LTB$_4$R1 (labeled with cytotracker green, shown as blue tracks) treated with CsH in a mixture with NS shRNA cells (labeled with cytotracker red, shown as red tracks) treated with DMSO (left) or MK866 (right). Composite graph shows displacement tracks of both types of cells. Speed and CI were calculated from the tracks of 40 cells and averaging over 4 independent movies. **(C)** Differentiated cells overexpressing the LTB$_4$R1 (labeled with cytotracker green, shown as blue tracks) in a mixture with Rab27a sh1 (labeled with cytotracker red, shown as red tracks) or SMPD2 sh2 (right) cells treated with DMSO. Composite graph shows displacement tracks of both types of cells. Speed and CI were calculated from the tracks of 40 cells and averaging over 4 independent movies. The symbols ***, **, *, and NS indicate $p < 0.0001$, $p < 0.001$, $p < 0.01$, and $p > 0.05$ respectively compared to CsH treated PLB-LTB$_4$R1 cells.

doi:10.1371/journal.pbio.1002336.g007

in lipid composition [35], we were able to separate exosomes from ectosomes using iodixanol density gradients. Moreover, the purified exosomes were able to activate resting neutrophils, indicating proinflammatory responses compared to the reported anti-inflammatory responses of ectosomes [34]. Finally, using Rab27a and SMPD2 KD cells, we established that exosomes represent the primary pathway for LTB$_4$ release in chemotaxing neutrophils under physiological stimulation conditions. Impaired neutrophil recruitment has been observed in Rab27a KO mice under in vivo neutrophil recruitment models [36]. Furthermore, neutrophils deficient in vesicle fusion show less migration in vitro and in an in vivo model of gout [37]. The migration defects we observed in Rab27a and SMPD2 KD cells therefore provide valuable mechanistic

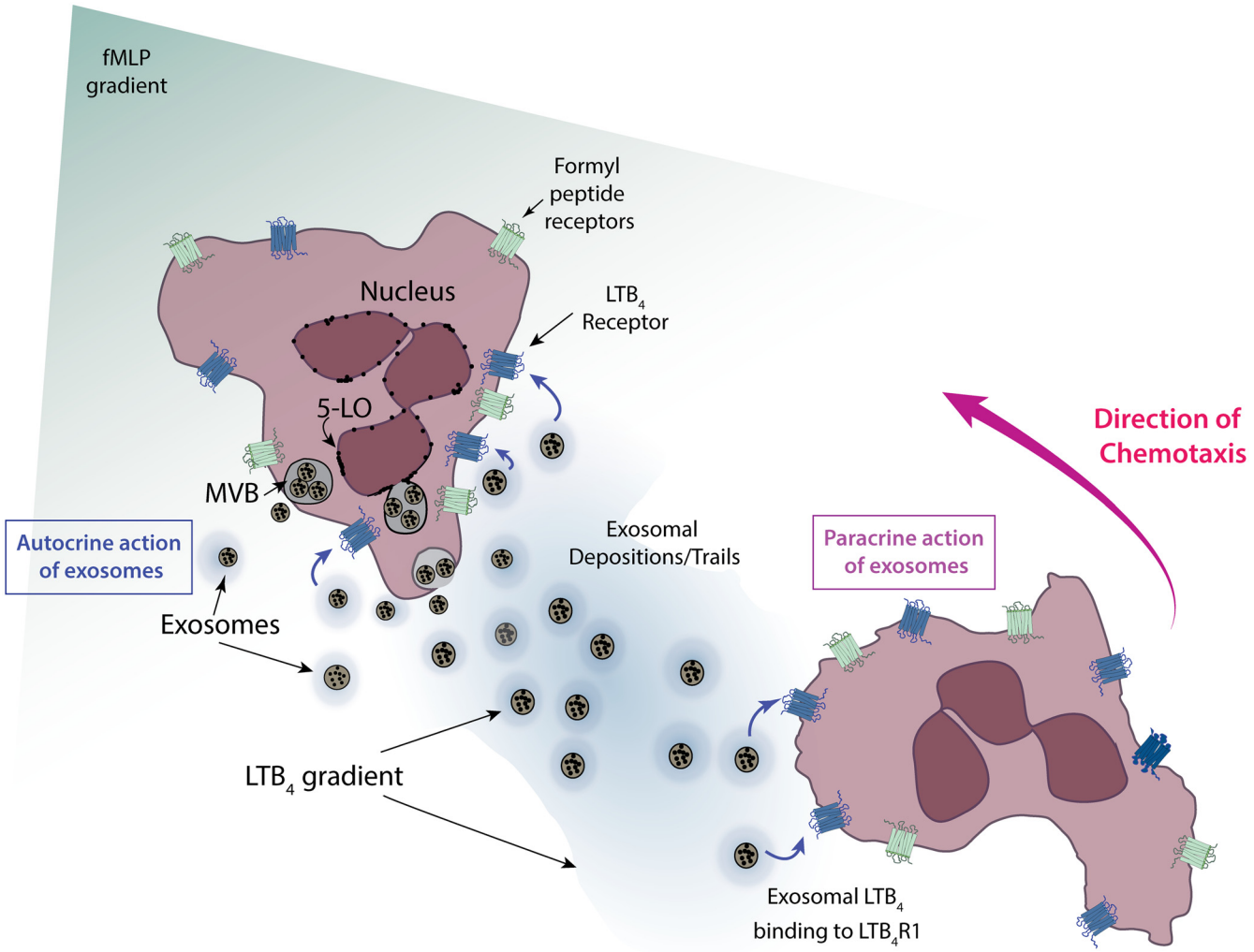

Fig 8. Illustration depicting exosome-mediated LTB$_4$ relay in neutrophils chemotaxing to fMLP. Cartoon depicting two neutrophils chemotaxing toward an fMLP gradient (green). LTB$_4$ released from exosomes are shown in blue. See text for details.

doi:10.1371/journal.pbio.1002336.g008

insights into the migration defects observed in vivo. Furthermore, the docking of 5-LO containing MVBs at the back of cells and the subsequent release of exosomes are reminiscent of the molecular beacon model first shown in chemotaxing *Dictyostelium* cells [17]. This is similar to recent in vivo observations made by Sung and colleagues [38], where exosomes released by HT1080 cells bind to integrins and act as adhesion trails for cellular guidance.

Under uniform stimulation conditions, exosomal LTB$_4$ levels range from 2–10 nM and are sufficient to elicit neutrophil migration in chemotaxis assays. This, however, may not reflect the actual amount of LTB$_4$ being released from exosomes during chemotaxis for the following reasons: (i) exosome release is fMLP dose-dependent and hence a function of the primary chemoattractant gradient; (ii) purified exosomes were prepared by uniformly stimulating neutrophils with subsaturating fMLP concentrations and losses incurred during the purification processes could lead to underestimated amounts of exosomes recovered; (iii) the rate of LTB$_4$ release from exosomes and the effective LTB$_4$ gradient across and between cells cannot be reliably measured in real time due to the lack of sensitive methodologies; and (iv) the presence of

the LTB_4 synthesizing enzymes, 5-LO, LTA_4H, and FLAP in neutrophil exosomes along with the presence of the primary substrate AA [39], suggest active exosomal LTB_4 synthesis. Indeed, exosomes isolated from dendritic cells are capable of synthesizing AA metabolites [32]. Although our study elucidates the trafficking and secretion of LTB_4 during neutrophil chemotaxis, the mechanisms regulating the release of exosomal LTB_4 remain to be determined. These may include membrane diffusion, passive or active lysis through released neutrophil proteases, or through docking to cell surface heparan sulfate proteoglycans [40]. Alternatively, active LTB_4 release may be mediated through ABC transporters [41] or other types of active processes. The availability of methods that are sensitive and, most importantly, capable of measuring LTB_4 in real time and space will help elucidate how LTB_4 gradients are established and propagated during neutrophil chemotaxis.

EM analyses on chemotaxing neutrophils provide key insights into the mechanisms that regulate LTB_4 synthesis and trafficking. In addition to its enrichment on the nuclear envelope, 5-LO is localized to the plasma membrane and to MVBs. Most interestingly, the 5-LO containing MVBs are often observed in close proximity to the nuclear envelope. The origination of MVBs from the nuclear envelope has previously been published [42,43]. Moreover, Record and colleagues have reported a close association of MVBs containing internalized exosomes with the nucleus in RBL-2H3 cells [39]. From these findings, we envision that the nuclear envelope represents a central hub for 5-LO distribution, leading to its segregation in two independent cellular pools: (i) the nucleus, where LTB_4 has been shown to bind to the peroxisome proliferator-activated receptor α [44] and regulate transcriptional responses and (ii) MVBs, where LTB_4 is destined to secretion and signal relay. We reason that the 5-LO plasma membrane labeling arises upon MVB fusion and release of exosomes into the extracellular environment. Our findings also bring into question the role of the canonical ESCRT-dependent exosomal biogenesis machinery in the synthesis and release of LTB_4-containing exosomes. Indeed, the fact that nSmase2 depletion results in a near complete inhibition of exosome release suggests that neutrophil exosome biogenesis predominantly relies on a ceramide-dependent and ESCRT-independent mechanism. Our observations are consistent with a study by Trajkovic et al. showing that secretion of CD63 in a mouse oligodendroglial cell line is blocked by a sphingomyelinase inhibitor, but not by a dominant-negative ESCRT component [30]. On the other hand, ESCRTIII, one of the key members of the ESCRT complex involved in ILV formation and MVB biogenesis, has recently been shown to localize at juxtanuclear regions that mediate the reformation of the nuclear envelope during cell division [45]. It hence remains to be determined whether the ESCRT machinery is involved in regulating the assembly of 5-LO-containing MVBs from the nuclear envelope during neutrophil chemotaxis.

Our findings show that exosomal LTB_4 regulates neutrophil chemotaxis in an autocrine and paracrine fashion. First, we found that Rab27a and SMPD2 KD cells as well as neutrophils treated with an nSmase2 inhibitor exhibit profound defects in directionality and recruitment range towards fMLP. Similar defects were observed in neutrophils derived from Rab27a KO mice [36] and were primarily attributed to granule exocytosis, a process that is closely related to exosome biogenesis and release. Chemotaxis has not been studied in neutrophils isolated from SMPD2 KO mice, although its role may be inferred through the effects of GW4869 on neutrophil migration. GW4869 did not inhibit neutrophil speed but abrogated directional migration towards fMLP [46], an observation that mirrors our own observation with GW4869 and SMPD2 KD cells. Second, we found that the defects in directionality and recruitment range of SMPD2 KD as well as GW4869-treated cells are rescued by the presence of control cells that provide exosomes to relay signals. One could argue that the rescue was simply due to supplementation of ceramide from the released exosomes and not related to LTB_4 content [46]. However, we observed a very similar phenotypical recovery by inhibiting LTB_4 synthesis

alone. More importantly, unlike control cells, the KD cells were unable to send a paracrine signal to neutrophils with blocked FPR1, clearly establishing that exosomes represent a critical bearer of the signal relay message.

Exosomes are well-established mediators of intercellular communication [47] and have been known to mediate cell migration in various systems [38]. This work establishes that exosomal communication is extremely efficient and critical in fast moving cells and occurs at a faster rate compared to the slow constitutive release of exosomes reported in the literature [29]. Moreover, our findings add valuable insight into the mechanisms that underlie chronic inflammatory conditions, such as asthma and rheumatoid arthritis [48], as well as lung cancer progression [49], where LTB_4 plays a central role. We envision that the secretion of other signals that foster communication between cells in harsh extracellular environments are similarly processed through exosome packaging.

Materials and Methods

Materials

OptiPrep, Histopaque 1077, fMLP, IL8, and LY294002 were obtained from Sigma-Aldrich (St. Louis, MO). LTB_4, MK886 and LY223982 were purchased from Cayman Chemical (Ann Arbor, MI). Anti-5-LO, Anti-p-Akt (clone C31E5E for S473), anti-AKT, anti-myosin light chain 2, anti-p-myosin light chain 2 (Ser19), anti-total ERK1/2, and anti-p-Erk1/2 (clone D13.14.4E) rabbit antibodies were all purchased from Cell Signaling Technology (Beverly, MA). Anti-MMP9, anti-MPO, anti-CD63, anti-LAMP1, and anti-GM130 were obtained from Abcam (Cambridge. MA). CD11b APC antibody was purchase from BD Biosciences (San Jose, CA).

Isolation of Human Peripheral Blood Neutrophils

Heparinized whole blood was obtained by venipuncture from healthy donors. Neutrophils were isolated using dextran sedimentation (3% dextran/0.9% NaCl) coupled to differential centrifugation over Histopaque 1077 [50]. Residual erythrocytes were removed using hypotonic lysis with 0.2% and 1.6% saline solutions.

Cell Lines

HEK293T cells (ATCC) and Phoenix cells (Orbigen, San Diego, CA) were maintained as previously described [51]. For virus packaging, 80% confluent cells were used for transient transfection using Lipofectamine reagent according to manufacturer's protocol (Life Technologies). PLB-985 cells were maintained in an undifferentiated state and differentiated as described [51]. The status of differentiation was monitored by Mac-1 staining.

Plasmid Constructs and Infections of PLB-985 Cells

PLB985 cells expressing mCherry-5LO and CD63-GFP as well as coexpressing both CD63-GFP and mCherry-5LO were created using a retroviral approach. Rab27a and SMPD2 KD were achieved using the pGIPZ lentiviral system (GE, Dharmacon).

Constructs and Infections of PLB-985 Cells

Retroviral approach. The mCherry gene was amplified from pCDNA3.1-mCherry, cloned at the 5' end of the 5-LO cDNA and introduced in pMSCV-Puro. Similarly, eGFP was amplified from pEGFP-N1, cloned at the 3' end of the CD63 cDNA (kindly donated by Dr. Paul Roche [NIH]), and introduced in pMSCV-Neo. Stable cell lines were created as described [51].

Briefly, expression plasmids were transfected along with the helper plasmid pVSV-G into the packaging Phoenix cell line using Lipofectamine 2000. Transiently produced viruses were harvested after 48 or 72 h. PLB-985 cells were infected with the virus with fresh RPMI1640 culture medium containing 4 μg/ml polybrene and incubated for an additional 48 hrs. Cells stably expressing the genes were selected in media containing 1.6 mg/ml G-418 or 0.8 μg/ml Puromycin. Stable clonal populations were generated after 14–21 d and maintained in the selection media. mCherry-5LO containing pMSCVneo was similarly infected into PLB-985 cells expressing CD63-GFP to create cells co-expressing CD63-GFP and mCherry-5LO.

Lentiviral approach. Undifferentiated PLB-985 cells were infected with pGIPZ shRNA lentiviruses (GE Dharmacon) carrying the hairpin sequences listed in the "Accession number" section using the manufacturer's recommendations. Of the six shRNA sequences tested targeting Rab27a and five sequences targeting SMPD2, two sequences each, namely, Rab27a shRNA1 (sh1), Rab27a shRNA3 (sh3), SMPD2 shRNA2 (sh2), and SMPD2 shRNA4 (sh4) were selected for further studies based on their ability to KD both mRNA and protein levels. pGIPZ nonsilencing lentiviral shRNA control was obtained from GE Dhramacon.

Exosome Isolation

5 x 10^8 cells were primed with GM-CSF (5 ng/ml; R&D Systems) for 30 min in RPMI without phenol red containing 5% FBS and 10 mM HEPES, centrifuged and resuspended in ice-cold PBS for 30 min to reduce basal exocytosis levels. Cells were harvested and resuspended in mHBSS with or without 2 nM fMLP for 30 min at 37°C and centrifuged at 500 xg for 5 min. To assess the exosome-producing ability of various stimulants, unprimed cells were resuspended in basal buffer (25 mM HEPES, pH 7.4, 140 mM NaCl, 4.7 mM KCl, 1.4 mM $MgCl_2$, and 10 mM glucose) and stimulated for 30 min with either ionomycin (1 μM) supplemented with $CaCl_2$ (2 mM), fMLP (1 μM), GM-CSF (5ng/ml), or DMSO (0.1%). The supernatant was further centrifuged at 2,000 xg for 20 min. The resulting supernatants were filtered twice through low protein-binding 0.45 μm filters and subsequently centrifuged at 100,000 xg for 60 min at 4°C. The recovered pellet, containing a heterogeneous mixture of crude vesicles, was resuspended in 500 μl PBS. Further purification of the exosomes was performed as previously reported [52]. Briefly, the resuspended vesicles were loaded onto a discontinuous gradient of iodixanol (40%, 20%, 10% and 5%, w/v solutions in 0.25 M sucrose/10 mM Tris, pH 7.5.), centrifuged at 100,000 xg for 18 h at 4°C. Fractions were collected, diluted in PBS, and centrifuged at 100,000 xg. The pellet was washed in PBS, and the recovered fractions were used as described.

Flow Cytometric Analysis of Exosomes

Purified exosomes were incubated with 3.9 μm diameter aldehyde/sulfate latex beads (Life Technologies) for 15 min at RT followed by the addition of 10 μg BSA for an additional 15 min. The incubation volume as increased to 250 μl in PBS and incubated overnight on a turnover rocker. The incubation was stopped the following day by adding glycine to a final concentration of 100 mM. The exosome-coated beads were washed twice in FACS wash (3% FCS and 0.1% NaN_3 in PBS) and resuspended in 400 μl FACS wash. The beads were incubated for 30 min with each conjugated primary antibody, washed and analyzed on a FACSCalibur flow cytometer (BD Biosciences). Bead-based flow cytometry was also performed with CD63 antibody-coated dynabeads according to manufacturer's protocol (Invitrogen).

Subcellular Fractionation through Nitrogen Cavitation

Freshly isolated neutrophils (50 x 10^6) were incubated with DFP for 15 min at 37°C, pelleted and resuspended in 1X Disruption Buffer (DB; 100 mM KCl, 3 mM NaCl, 3.5 mM $MgCl_2$, 1.5

mM EGTA, and 10mM 1,4-piperazinediethanesulfonic acid (PIPES), pH 7.2, including 1 mM sodium salt of ATP, and 0.5 M PMSF) with or without 2 nM fMLP. The reaction was stopped after 2 min by adding an equal volume of ice-cold DB. Cavitation was carried out for 5 min at 500 psi on ice. Cavitates were collected and EGTA was added to the final concentration of 1.5 mM. Lysed cells were centrifuged at 400 xg for 20 min to remove cell debris and nuclei and 15,000 xg for 15 min to remove mitochondria. The supernatant was then top loaded onto a 5%–30% continuous OptiPrep gradient prepared by appropriately diluting a 60% optiprep stock with 3X disruption buffer. The gradient was centrifuged at 34,000 xg for 18.5 h, and 1 ml fractions were collected. Fractionates < 1.04 g/l containing primarily cytosolic fraction were discarded and the rest analyzed by immunoblotting after TCA (Trichloroacetic acid) precipitation. To determine the density of each fraction, a control OptiPrep gradient containing a blank containing disruption buffer was run in parallel. Fractions were collected as described, serially diluted 1:10,000 with water, and the iodixanol concentration determined by absorbance at 244 nm using a molar extinction coefficient of 320 L $g^{-1}cm^{-1}$.

Chemotaxis Assays

Chemotaxis was assessed using the under-agarose assay or the EZ-Taxiscan as previously described [51,53].

Under-agarose assay. Cell culture dishes were coated with 0.2% gelatin in PBS for 1 h at 37°C. 0.5% agarose in 50% PBS—50% mHBSS was poured and allowed to solidify for 40 min. Three 1 mm diameter wells were carved at 2 mm distance from each other. A chemoattractant was placed in the middle well 15 min before plating neutrophils. The chemoattractant concentration achieved using this method was assessed as described by Afonso et al. [6]. Typically, a gradient of 50 pM/μm fMLP was used for under-agarose assays. 5 x 10^5 neutrophils in 5 μL mHBSS were plated in the outer wells and incubated at 37°C. Cells were allowed to chemotax for 30 min to 2 h depending on the experimental requirement. Cells migrating under-agarose were imaged using Axiovert 200 (Carl Zeiss, Inc.) equipped with a confocal system (Ultraview ERS; PerkinElmer) with a spinning disk head (Yokogawa). Single plane images and z stacks were taken using 63 and 100× plan neofluor objectives (Carl Zeiss, Inc.).

EZ-Taxiscan Assay. The EZ-Taxiscan chamber (Effector Cell Institute, Tokyo, Japan) was assembled as described by the manufacturer. Cell migration was recorded every 15 s for 45 min at 37°C in a humidified environmental chamber. Coverslips and chips used in the chamber were coated with 1% bovine serum albumin at room temperature for 1 h. All glass coverslips were ultrasonicated and washed before use. Cell migration analysis was conducted using MATLAB software as previously described [51].

Adhesion Assay

Cells (5 x 10^5 cells/well) were plated on 96-well plates coated with fibronectin, stimulated for 30 min at 37°C, shaken at 2,000 RPM (radius = 1 cm) for 10 s on an orbital shaker, and unbound cells were removed. The remaining cells were fixed (4% PFA) and stained with crystal violet 5 mg/mL in 2% ethanol. Crystal violet was extracted by the addition of 2% SDS and absorbance was measured at 570 nm.

EM Analyses

Neutrophils were allowed to migrate under-agarose towards an fMLP gradient for 1 hr after which the agarose was removed and the cells were fixed in 0.1 M cacodylate buffer pH 7.4, containing 5% sucrose, 4% paraformaldehyde, and 0.1% glutaradehyde for 2 h at 22°C. The cells were blocked and permeablized in PBS + 5% BSA, 0.1% NaN_3, and 0.1% saponin, followed by

the addition of 5-LO antibody or a control rabbit antibody, and subsequently with rabbit secondary antibody conjugated to nanogold (4 nm; Nanoprobes). The cells are fixed with 2.5% glutaraldehyde followed by gold enhancement of the nanogold particles (Nanoprobes), osmium tetroxide staining, and epoxy block preparation. Immunoelectron staining was performed on thin cut block sections (EML, NCI) using Hitachi H7600 Transmission electron microscope. MVBs with greater than 5 immunogold particle/μm were considered 5-LO positive MVBs for quantification purposes. In separate experiments, uranyl acetate negative-stain immuno-EM was performed to analyze the size and number of purified exosome samples.

Mixed Cell Chemotaxis Assay, Image Acquisition and Motility Analysis

Cytotracker dyes were added to differentiated PLB-985 cells or freshly isolated neutrophils according to manufacturer's protocol (Life Technologies), washed and resuspended in modified HBSS (mHBSS) containing appropriate inhibitors/antagonists. Cells were then washed and 2.5 x 10^5 cells of differently labeled cells were mixed. These cells were resuspended in 5 μl mHBSS and loaded onto an under-agarose chamber. Time-lapse imaging was performed using a Plan-Neofluar 10x/0.30 objective (Zeiss Axiovert S100 microscope). Cell tracks were extracted and analyzed using a method developed by McCann et al. [54] supplemented by tracking through ImageJ. CI and Δα (persistance) were used to analyze motility behavior. CI was calculated by taking the cosine of the angle between the final displacement vector and the line connecting the chemotactic source to the initial position of the cell. A value of 1 designates perfect chemotaxis. Δα is measured through the angular change between the displacement vector at any given time and the preceding displacement vector. Larger Δα designates lower persistence.

LTB_4 Measurements

Total LTB_4 levels were measured using an ELISA kit (R&D Systems). Briefly, neutrophils or PLB-985 cells were resuspended at 1 x 10^6 cells/ml in PBS and incubated for 30 min on ice. GM-CSF (5 ng/ml; R&D Systems) was added and cells were further incubated for 1 hr at 37°C, centrifuged at 400 xg for 5 min, resuspended in a volume of 200 μl at 24 x 10^6 cells/ml in RPMI and incubated at 37°C until stimulated. The reactions were stopped by adding cold PBS. Cells were centrifuged and LTB_4 in supernatants were assayed according to manufacturer's instructions. Exosomal LTB_4 was measured using the EIA kit according to manufacturer's protocol (Cayman Chemicals) after disruption by sonication. To measure LTB_4 in the vesicular fractions of lysed neutrophils, total lipids were first extracted from the different fractions using a method outlined by McColl et al. [55]. The extracted lipids were acidified to pH 4.0 loaded onto a C18 SPE column and eluted with ethyl acetate containing 10% methanol, evaporated under inert nitrogen stream and resuspended in buffer to obtain a concentrated pool of LTB_4. LTB_4 levels were measured using the EIA kit (Cayman chemicals) according to manufacturer's recommendations.

Immunoblotting

Neutrophils were either resuspended in RPMI (1% bovine serum) or plated on fibronectin-coated chambers (for pMLCII) and incubated with inhibitors and diisopropyl fluorophosphates (DFP) (2 mM) for 10 min at 37°C. Cells were then stimulated with fMLP, collected at specific time points, lysed for 15 min in ice-cold lysis buffer (20 mM Tris pH 7.5, 10 mN NaCl, 1 mM EDTA, 0.1% NP-40, 3 mM DFP, 2 mM orthovanadate, 10 g/mL aprotinin, 10 g/mL leupeptin, 2.5 mM napyrophosphate, Complete Protease Inhibitor cocktail [Roche Diagnostics, Indianapolis, IN]), and processed for SDS-PAGE analyses.

Accession Numbers

XM_005267109 (SMPD2 shRNA1):
TGCTGTTGACAGTGAGCGCCGCCGTTGATGTGTGTGCTAATAGTGAAGCCACAG
ATGTATTAGCACACACATCAACGGCGATGCCTACTGCCTCGGA
XM_005267109 (SMPD2 shRNA2):
TGCTGTTGACAGTGAGCGCAGGCAACACAATGGTACCCAATAGTGAAGCCACA
GATGTATTGGGTACCATTGTGTTGCCTTTGCCTACTGCCTCGGA
NM_003080 (SMPD2 shRNA3):
TGCTGTTGACAGTGAGCGAGGGGACAGAACTAAAGAACAATAGTGAAGCCACA
GATGTATTGTTCTTTAGTTCTGTCCCCCTGCCTACTGCCTCGGA
XM_005267109 (SMPD2 shRNA4):
TGCTGTTGACAGTGAGCGCCCGCATTGACTACGTGCTTTATAGTGAAGCCACAG
ATGTATAAAGCACGTAGTCAATGCGGATGCCTACTGCCTCGGA
NM_003080 (SMPD2 shRNA5):
TGCTGTTGACAGTGAGCGATGGGTTTTACATCTCCTGTAATAGTGAAGCCACAG
ATGTATTACAGGAGATGTAAAACCCAGTGCCTACTGCCTCGGA
NM_004580 (Rab27a shRNA1):
TGCTGTTGACAGTGAGCGCGCTCAATGTCTTTGAGTATTATAGTGAAGCCACAG
ATGTATAATACTCAAAGACATTGAGCTTGCCTACTGCCTCGGA
NM_183236 (Rab27a shRNA2):
TGCTGTTGACAGTGAGCGAGCCCAGAGTCTTACATTTAAGTAGTGAAGCCACAG
ATGTACTTAAATGTAAGACTCTGGGCCTGCCTACTGCCTCGGA
NM_004580 (Rab27a shRNA3):
TGCTGTTGACAGTGAGCGCGGCTGCAGCTTTATTAGCTTATAGTGAAGCCACAG
ATGTATAAGCTAATAAAGCTGCAGCCTTGCCTACTGCCTCGGA
XM_005254577 (Rab27a shRNA4):
TGCTGTTGACAGTGAGCGCCCAGTGTACTTTACCAATATATAGTGAAGCCACAG
ATGTATATATTGGTAAAGTACACTGGTTGCCTACTGCCTCGGA
NM_183234 (Rab27a shRNA5):
TGCTGTTGACAGTGAGCGCAGGGAAGACCAGTGTACTTTATAGTGAAGCCACAG
ATGTATAAAGTACACTGGTCTTCCCTATGCCTACTGCCTCGGA
NM_183236 (Rab27a shRNA6):
TGCTGTTGACAGTGAGCGAATGCCTCTACGGATCAGTTAATAGTGAAGCCACAG
ATGTATTAACTGATCCGTAGAGGCATGTGCCTACTGCCTCGGA

Supporting Information

S1 Data. Raw data for all quantitative analyses in the main figures. Raw values for Figs 1A and 1B, 2F, 3D, 3F, 3I, 4A and 4B, 5A–5D, 6A–6C and 7A–7C are presented. The data are shown for each figure panel in a separate worksheet.
(XLSX)

S2 Data. Excel file containing raw data for supplemental figures. S2A, S2B, and S2D, S3A–S3C, S4C, S5A, S6A and S6B and S7A and S7B Figs.
(XLSX)

S1 Fig. Characterization of cells expressing CD63-GFP, mCherry-5LO, and CD63/5-LO. **(A)** PLB-985 cells expressing CD63-GFP or mCherry-5LO were plated on fibronectin-coated (50 μg/ml) coverslips, fixed with 4% paraformaldehyde, and imaged in the absence of fMLP. Also see S1 Movie. **(B)** PLB985 cells expressing mCherry-5LO migrating under-agarose

towards fMLP were fixed with 3.7% paraformaldehyde, 0.1% glutaraldehyde in 0.1 M cacodylate buffer containing 320 mM sucrose, permeablized with 0.2% Triton-X100 for 2 min and counterstained with Phalloidin FITC. The slope of the gradient is ~50 pM/μm, as previously assessed [6]. **(C)** Images of PLB985 cells expressing CD63-GFP migrating under-agarose towards fMLP. The slope of the gradient is ~50 pM/μm, as previously assessed [6]. Images shown are representative of six independent experiments
(TIF)

S2 Fig. Characterization of exosomes released from resting and activated neutrophils. (A) Exosomes were purified from neutrophils treated with increasing concentrations of fMLP and their surface levels of CD11b assessed by bead-based flow cytometry. Percentage positivity shown is based on the gated exosome fraction derived from nonstimulated cells. Inset: Amount of purified exosomes is quantified by multiplying the percentage positivity of each fraction from four independent experiments with corresponding relative median fluorescence intensity values. **(B)** CD81 levels in exosomes purified from neutrophils treated with increasing concentrations of fMLP assessed as mentioned in A. **(C)** CD81 levels in exosomes purified from neutrophils treated with DMSO, Ionomycin, fMLP, and GM-CSF. **(D)** Quantitation of exosome amounts were done as descried in A, using values from three independent experiments.
(TIF)

S3 Fig. Bioactivity of purified exosomes. (A) LTB_4 (10nM) or exosomes isolated from PLB-985 cells expressing either mCherry or mCherry-5LO (50 μg/ml) was added to neutrophils for 15 min and pAkt (S473) and p44/42 MAPK (Erk1/2; T202/Y204) levels were measured using specific antibodies. Quantification of three independent experiments is presented as the amount of phosphorylated protein relative to that of DMSO-treated cells (mean ± SD). The amount of pAkt or pErk1/2 at each point was standardized by dividing its value with the value of total Akt or Erk1/2 at the same time point. **(B)** Neutrophils were treated with or without 10 μM LY223982 for 30 min and allowed to migrate towards 1 μM fMLP. Data are representative of three independent experiments. See legend of Fig 4E for details. **(C)** Exosomal LTB_4 (See legends of Fig 4G for details) derived from PLB-985 cells expressing mCherry, mCherry-5LO or CD63-GFP was added to neutrophils (pretreated or not with LY223982) for 15 min and pAkt (S473) levels were measured using specific antibodies. Quantification of three independent experiments is presented as the amount of pAkt S473 after stimulation relative to that of unstimulated cells (mean ± SD). The amount of pAkt S473 at each time point was standardized by dividing its value with the value of total Akt of the same time point.
(TIF)

S4 Fig. Characterization of Rab27a and SMPD2 KD cells. (A) Differentiated and undifferentiated PLB-985 cells were lysed and subjected to western analyses using antibodies specific for Rab27a and nSmase2. GAPDH levels were used as loading controls. Results are representative of three independent experiments. **(B)** Exosomes were purified from differentiated control (NS shRNA), Rab27a shRNA (sh1; sh3), or SMPD2 shRNA (sh2; sh4) KD cells after treatment with fMLP (2 nM, 30 min) and analyzed using a bead-based flow cytometry assay with CD63-FITC, CD81-PE, and CD11b-APC conjugated antibodies. See Fig 5A for quantification and additional details. **(C)** Differentiated NS shRNA, Rab27a or SMPD2 KD cells or PLB-985 cells over-expressing LTB_4R1 were plated on fibronectin-coated plates for 10 min and uniformly stimulated uniformly with 1 nM fMLP. At specific time points, samples were subjected to western analyses using an antibody against pMLCII and total MLCII. Quantification of three independent experiments is presented as the amount of pMLCII after fMLP stimulation relative to

that at time 0 (mean ± SD).
(TIF)

S5 Fig. Response of Rab27a and SMPD2 KD cells to fMLP. (A) Differentiated PLB-985 Rab27a and SMPD2 KD cells were plated on fibronectin-coated (50 μg/ml) plates for 10 min and uniformly stimulated with 1 μM fMLP. The plates were then shaken, and the number of remaining cells attached to the plates was estimated by crystal violet staining. Results represent the percent average ± SD compared to PLB-985 control of four independent experiments. **(B)** Differentiated PLB-985, NSshRNA, Rab27a, and SMPD2 KD cells were uniformly stimulated with 100 nM fMLP and pERK1/2 levels were assessed by immunoblotting. **(C)** EZ-Taxiscan chemotaxis towards 1 μM of control and KD cell lines. Corresponding migration speeds and CI were calculated from four different experiments and represented as mean ± SD. See legend of Fig 4E for details. Also see S9 Movie.
(TIF)

S6 Fig. Effect of SMPD2 KD on exosome production and neutrophil chemotaxis. (A) Exosomes purified from DMSO- or GW4869-treated neutrophils were incubated with anti-CD63 antibody-coated Dynabeads (Invitrogen) and detected using CD81-PE antibody in a bead-based flow cytometry assay. Inset: Inhibition was quantified using the relative median fluorescence intensity values from four independent experiments. **(B)** Representative tracks of chemotaxing differentiated PLB-985 cells under-agarose towards a 50 pM/μm gradient of fMLP. Top left: NS shRNA cells stained with cytotracker red. Bottom left: SMPD2 sh1 cells stained with cytotracker red. Top Right: NSshRNA cells stained with cytotracker green in a mixture of SMPD2sh1 and NSshRNA cells. Bottom Right: SMPD2 sh1 cells stained with cytotracker red in a mixture of SMPD2 sh1 and NSshRNA cells. The temporal location of cells in the X- or Y-direction is coded according to the colormap. Also see Fig 6A and 6B for further details.
(TIF)

S7 Fig. Paracrine action of exosomes on neutrophil chemotaxis. (A) Representative tracks, speed and CI of mixtures of cytotracker-labeled neutrophils treated with DMSO or CsH migrating under-agarose towards a ~50 pM/μm gradient of fMLP. (B) Representative tracks, speed and CI of mixtures of cytotracker-labeled neutrophils treated with CsH, MK886 or GW4869 migrating under-agarose towards a ~50 pM/μm gradient of fMLP. Speed and CI were calculated from the tracks of 40 cells and averaging over 4 independent movies.
(TIF)

S1 Movie. Localization of 5-LO in unstimulated mCherry-5LO cells. Differentiated cells expressing mCherry-5LO were plated on fibronectin-coated coverslips. Images were acquired every 30 s for 18 min.
(AVI)

S2 Movie. Localization of 5-LO in mCherry-5LO cells uniformly stimulated with fMLP. Differentiated PLB-985 cells expressing mCherry-5LO were plated on fibronectin-coated coverslips and uniformly stimulated with 10 nM fMLP. Images were acquired every 30 s for 5 min.
(AVI)

S3 Movie. Redistribution of 5-LO in mCherry-5LO cells chemotaxing under-agarose towards fMLP. Differentiated PLB-985 cells expressing mCherry-5LO were allowed to chemotax under-agarose towards fMLP gradient on a coverslip coated with 0.2% gelatin. Time lapse images were acquired every 30 s for 5 min, 700 μm from away from the chemoattractant well.

The movie represents a single Z-slice at 1.5 μm. Gradient slope ~ 50 pM/μm.
(AVI)

S4 Movie. Colocalization of mCherry-5-LO and CD63-GFP in cells chemotaxing under-agarose towards fMLP. Differentiated PLB-985 cells were allowed to chemotax under-agarose towards fMLP gradient on a coverslip coated with 0.2% gelatin. Time lapse images were acquired every 10 s for 4 min, 700 μm from away from the chemoattractant well The movie represents a single Z-slice at 1.5 μm above coverslip. Gradient slope ~ 50 pM/μm.
(AVI)

S5 Movie. Neutrophil chemotaxis towards fMLP, LTB_4 or exosomes. EZ-Taxiscan chemotaxis of neutrophils moving towards fMLP (10 nM), LTB_4 (100 nM), exosomes (100 μg/ml) or a buffer control. Images were acquired every 15 s for 60 min.
(MP4)

S6 Movie. Neutrophil chemotaxis towards LTB_4 or exosomes in the presence or absence of an LTB_4R1 antagonist. EZ-Taxiscan chemotaxis of neutrophils moving towards LTB_4 (100 nM) or exosomes (50 μg/ml). Cells were treated with either DMSO or the LTB_4R1 antagonist LY223982. Images were acquired every 15 s for 60 min.
(MP4)

S7 Movie. Neutrophils chemotaxis towards exosomes purified from MK886-treated cells. EZ-Taxiscan chemotaxis of neutrophils chemotaxing towards 100 μg/ml exosomes purified from DMSO- or MK886-treated cells expressing mCherry-5LO. Images were acquired every 15 s for 50 min.
(MP4)

S8 Movie. Chemotaxis of Rab27a and SMPD2 KD cells towards fMLP. EZ-Taxiscan chemotaxis of differentiated PLB-985 NSshRNA, Rab27ash1, Rab27ash3, SMPD2sh2 or SMPD2sh4 cells chemotaxing towards 1 nM fMLP. Images were acquired every 15 s for 30 min.
(MP4)

S9 Movie. Chemotaxis of Rab27a and SMPD2 KD cells towards fMLP. EZ-Taxiscan chemotaxis of differentiated PLB-985 NSshRNA, Rab27ash1, Rab27ash3, SMPD2sh2, and SMPD2sh4 cells moving towards 1 μM fMLP. Images were acquired every 15 s for 45 mins.
(MP4)

S10 Movie. Chemotaxis of MK886-treated neutrophils in the presence of untreated neutrophils. DMSO-treated neutrophils, stained with cytotracker red (left panel), MK886-treated neutrophils stained with cytotracker red (middle panel) and mixed populations of DMSO-treated neutrophils stained green and MK886-treated neutrophils stained red (right panel) were allowed to migrate under-agarose towards fMLP gradient on a coverslip coated with 0.2% gelatin. Gradient slope ~ 50 pM/μm. Images were acquired every 60 s for 40 min.
(MP4)

S11 Movie. Chemotaxis of GW4869-treated neutrophils in the presence of untreated neutrophils. DMSO-treated neutrophils stained with cytotracker red (left panel), GW4869-treated neutrophils stained with cytotracker red (middle panel) and mixed populations of DMSO-treated neutrophils stained green and GW4869-treated neutrophils stained red (right panel) were allowed to migrate under-agarose towards fMLP gradient on a coverslip coated with 0.2% gelatin. Gradient slope ~ 50 pM/μm. Images were acquired every 60 s for 40 min.
(MP4)

S12 Movie. Paracrine action of exosomes during neutrophil chemotaxis. Neutrophils stained with cytotracker green and treated with DMSO or CsH were mixed with inhibitor- or control-treated neutrophils stained with cytotracker red. The mixed cells were allowed to chemotax under-agarose towards fMLP on a coverslip coated with 0.2% gelatin. Images were acquired every 60 s for 60 min.
(MP4)

Acknowledgments

We thank the NIH Blood Bank for providing human blood from healthy volunteers. We are grateful to Dr. Paul Roche (NIH) for providing the CD63 cDNA and Dr. Konstadinos Moissoglu (NIH) for generating the LTB_4R1 expressing PLB-985 cells. We also thank the Parent laboratory members, in particular Drs. Kataria, Kriebel, Stuelten, and Subramanian, for excellent discussions and suggestions and for valuable input on the manuscript.

Author Contributions

Conceived and designed the experiments: RM CAP. Performed the experiments: RM ATT. Analyzed the data: RM CAP. Wrote the paper: RM CAP.

References

1. Jin T, Xu X, Hereld D (2008) Chemotaxis, chemokine receptors and human disease. Cytokine 44: 1–8. doi: 10.1016/j.cyto.2008.06.017 PMID: 18722135
2. Kolaczkowska E, Kubes P (2013) Neutrophil recruitment and function in health and inflammation. Nat Rev Immunol 13: 159–175. doi: 10.1038/nri3399 PMID: 23435331
3. Majumdar R, Sixt M, Parent CA (2014) New paradigms in the establishment and maintenance of gradients during directed cell migration. Curr Opin Cell Biol 30: 33–40. doi: 10.1016/j.ceb.2014.05.010 PMID: 24959970
4. Mahadeo DC, Parent CA (2006) Signal relay during the life cycle of *Dictyostelium*. Curr Top Dev Biol 73: 115–140. PMID: 16782457
5. Gouwy M, De Buck M, Portner N, Opdenakker G, Proost P, et al. (2015) Serum amyloid A chemoattracts immature dendritic cells and indirectly provokes monocyte chemotaxis by induction of cooperating CC and CXC chemokines. Eur J Immunol 45: 101–112. doi: 10.1002/eji.201444818 PMID: 25345597
6. Afonso PV, Janka-Junttila M, Lee YJ, McCann CP, Oliver CM, et al. (2012) LTB_4 is a signal-relay molecule during neutrophil chemotaxis. Dev Cell 22: 1079–1091. doi: 10.1016/j.devcel.2012.02.003 PMID: 22542839
7. Needleman P, Turk J, Jakschik BA, Morrison AR, Lefkowith JB (1986) Arachidonic acid metabolism. Annu Rev Biochem 55: 69–102. PMID: 3017195
8. Chou RC, Kim ND, Sadik CD, Seung E, Lan Y, et al. (2010) Lipid-cytokine-chemokine cascade drives neutrophil recruitment in a murine model of inflammatory arthritis. Immunity 33: 266–278. doi: 10.1016/j.immuni.2010.07.018 PMID: 20727790
9. McDonald B, Kubes P (2010) Chemokines: sirens of neutrophil recruitment-but is it just one song? Immunity 33: 148–149. doi: 10.1016/j.immuni.2010.08.006 PMID: 20732637
10. Oyoshi MK, He R, Li Y, Mondal S, Yoon J, et al. (2012) Leukotriene B_4-driven neutrophil recruitment to the skin is essential for allergic skin inflammation. Immunity 37: 747–758. doi: 10.1016/j.immuni.2012.06.018 PMID: 23063331
11. Lammermann T, Afonso PV, Angermann BR, Wang JM, Kastenmuller W, et al. (2013) Neutrophil swarms require LTB_4 and integrins at sites of cell death *in vivo*. Nature 498: 371–375. doi: 10.1038/nature12175 PMID: 23708969
12. Uden AM, Hafstrom I, Palmblad J (1986) Relation to chemotactic factor gradients to neutrophil migration and orientation under agarose. J Leukoc Biol 39: 27–35. PMID: 3001211
13. Iwahashi M, Kasahara Y, Matsuzawa H, Yagi K, Nomura K, et al. (2000) Self-diffusion, dynamical molecular conformation, and liquid structures of n-saturated and unsaturated fatty acids. Journal of Physical Chemistry B 104: 6186–6194. doi: 10.1021/jp000610l

14. Zsila F, Bikadi Z, Lockwood SF (2005) *In vitro* binding of leukotriene B_4 (LTB_4) to human serum albumin: evidence from spectroscopic, molecular modeling, and competitive displacement studies. Bioorg Med Chem Lett 15: 3725–3731. PMID: 15993588

15. Greco V, Hannus M, Eaton S (2001) Argosomes: a potential vehicle for the spread of morphogens through epithelia. Cell 106: 633–645. PMID: 11551510

16. Entchev EV, Gonzalez-Gaitan MA (2002) Morphogen gradient formation and vesicular trafficking. Traffic 3: 98–109. PMID: 11929600

17. Kriebel PW, Barr VA, Rericha EC, Zhang G, Parent CA (2008) Collective cell migration requires vesicular trafficking for chemoattractant delivery at the trailing edge. J Cell Biol 183: 949–961. doi: 10.1083/jcb.200808105 PMID: 19047467

18. Faurschou M, Borregaard N (2003) Neutrophil granules and secretory vesicles in inflammation. Microbes Infect 5: 1317–1327. PMID: 14613775

19. Kobayashi T, Vischer UM, Rosnoblet C, Lebrand C, Lindsay M, et al. (2000) The tetraspanin CD63/lamp3 cycles between endocytic and secretory compartments in human endothelial cells. Mol Biol Cell 11: 1829–1843. PMID: 10793155

20. Cieutat AM, Lobel P, August JT, Kjeldsen L, Sengelov H, et al. (1998) Azurophilic granules of human neutrophilic leukocytes are deficient in lysosome-associated membrane proteins but retain the mannose 6-phosphate recognition marker. Blood 91: 1044–1058. PMID: 9446668

21. Luo M, Jones SM, Peters-Golden M, Brock TG (2003) Nuclear localization of 5-lipoxygenase as a determinant of leukotriene B_4 synthetic capacity. Proc Natl Acad Sci U S A 100: 12165–12170. PMID: 14530386

22. Denzer K, Kleijmeer MJ, Heijnen HF, Stoorvogel W, Geuze HJ (2000) Exosome: from internal vesicle of the multivesicular body to intercellular signaling device. J Cell Sci 113 Pt 19: 3365–3374. PMID: 10984428

23. Andreu Z, Yanez-Mo M (2014) Tetraspanins in extracellular vesicle formation and function. Front Immunol 5: 442. doi: 10.3389/fimmu.2014.00442 PMID: 25278937

24. Tucker KA, Lilly MB, Heck L Jr., Rado TA (1987) Characterization of a new human diploid myeloid leukemia cell line (PLB-985) with granulocytic and monocytic differentiating capacity. Blood 70: 372–378. PMID: 3475136

25. Raposo G, Stoorvogel W (2013) Extracellular vesicles: exosomes, microvesicles, and friends. J Cell Biol 200: 373–383. doi: 10.1083/jcb.201211138 PMID: 23420871

26. Hess C, Sadallah S, Hefti A, Landmann R, Schifferli JA (1999) Ectosomes released by human neutrophils are specialized functional units. J Immunol 163: 4564–4573. PMID: 10510400

27. Lancaster GI, Febbraio MA (2005) Exosome-dependent trafficking of HSP70: a novel secretory pathway for cellular stress proteins. J Biol Chem 280: 23349–23355. PMID: 15826944

28. Ostrowski M, Carmo NB, Krumeich S, Fanget I, Raposo G, et al. (2010) Rab27a and Rab27b control different steps of the exosome secretion pathway. Nat Cell Biol 12: 19–30; sup pp 11–13. doi: 10.1038/ncb2000 PMID: 19966785

29. Bobrie A, Krumeich S, Reyal F, Recchi C, Moita LF, et al. (2012) Rab27a supports exosome-dependent and -independent mechanisms that modify the tumor microenvironment and can promote tumor progression. Cancer Res 72: 4920–4930. doi: 10.1158/0008-5472.CAN-12-0925 PMID: 22865453

30. Trajkovic K, Hsu C, Chiantia S, Rajendran L, Wenzel D, et al. (2008) Ceramide triggers budding of exosome vesicles into multivesicular endosomes. Science 319: 1244–1247. doi: 10.1126/science.1153124 PMID: 18309083

31. Stenfeldt A-L, Karlsson J, Wennerås C, Bylund J, Fu H, et al. (2007) Cyclosporin H, Boc-MLF and Boc-FLFLF are antagonists that preferentially inhibit activity triggered through the formyl peptide receptor. Inflammation 30: 224–229. PMID: 17687636

32. Esser J, Gehrmann U, D'Alexandri FL, Hidalgo-Estevez AM, Wheelock CE, et al. (2010) Exosomes from human macrophages and dendritic cells contain enzymes for leukotriene biosynthesis and promote granulocyte migration. J Allergy Clin Immunol 126: 1032–1040, 1040 e1031–1034. doi: 10.1016/j.jaci.2010.06.039 PMID: 20728205

33. Schorey JS, Cheng Y, Singh PP, Smith VL (2015) Exosomes and other extracellular vesicles in host-pathogen interactions. EMBO Rep 16: 24–43. doi: 10.15252/embr.201439363 PMID: 25488940

34. Gasser O, Schifferli JA (2004) Activated polymorphonuclear neutrophils disseminate anti-inflammatory microparticles by ectocytosis. Blood 104: 2543–2548. PMID: 15213101

35. Sadallah S, Eken C, Schifferli JA (2011) Ectosomes as modulators of inflammation and immunity. Clin Exp Immunol 163: 26–32. doi: 10.1111/j.1365-2249.2010.04271.x PMID: 21039423

36. Singh RK, Liao W, Tracey-White D, Recchi C, Tolmachova T, et al. (2012) Rab27a-mediated protease release regulates neutrophil recruitment by allowing uropod detachment. J Cell Sci 125: 1652–1656. doi: 10.1242/jcs.100438 PMID: 22375060

37. Colvin RA, Means TK, Diefenbach TJ, Moita LF, Friday RP, et al. (2010) Synaptotagmin-mediated vesicle fusion regulates cell migration. Nat Immunol 11: 495–502. doi: 10.1038/ni.1878 PMID: 20473299

38. Sung BH, Ketova T, Hoshino D, Zijlstra A, Weaver AM (2015) Directional cell movement through tissues is controlled by exosome secretion. Nat Commun 6: 7164. doi: 10.1038/ncomms8164 PMID: 25968605

39. Subra C, Grand D, Laulagnier K, Stella A, Lambeau G, et al. (2010) Exosomes account for vesicle-mediated transcellular transport of activatable phospholipases and prostaglandins. J Lipid Res 51: 2105–2120. doi: 10.1194/jlr.M003657 PMID: 20424270

40. Christianson HC, Svensson KJ, van Kuppevelt TH, Li JP, Belting M (2013) Cancer cell exosomes depend on cell-surface heparan sulfate proteoglycans for their internalization and functional activity. Proc Natl Acad Sci U S A 110: 17380–17385. doi: 10.1073/pnas.1304266110 PMID: 24101524

41. Rius M, Hummel-Eisenbeiss J, Keppler D (2008) ATP-dependent transport of leukotrienes B_4 and C_4 by the multidrug resistance protein ABCC4 (MRP4). J Pharmacol Exp Ther 324: 86–94. PMID: 17959747

42. Conti CJ, Klein-Szanto AJ (1973) Nuclear multivesicular bodies in cultured hamster cells. Experientia 29: 850–851. PMID: 4724723

43. Kilarski W, Jasinski A (1970) The formation of multivesicular bodies from the nuclear envelope. J Cell Biol 45: 205–211. PMID: 4327571

44. Devchand PR, Keller H, Peters JM, Vazquez M, Gonzalez FJ, et al. (1996) The PPARα-leukotriene B_4 pathway to inflammation control. Nature 384: 39–43. PMID: 8900274

45. Olmos Y, Hodgson L, Mantell J, Verkade P, Carlton JG (2015) ESCRT-III controls nuclear envelope reformation. Nature 522: 236–239. doi: 10.1038/nature14503 PMID: 26040713

46. Sitrin RG, Sassanella TM, Petty HR (2011) An obligate role for membrane-associated neutral sphingomyelinase activity in orienting chemotactic migration of human neutrophils. Am J Respir Cell Mol Biol 44: 205–212. doi: 10.1165/rcmb.2010-0019OC PMID: 20378749

47. Simons M, Raposo G (2009) Exosomes—vesicular carriers for intercellular communication. Current opinion in cell biology 21: 575–581. doi: 10.1016/j.ceb.2009.03.007 PMID: 19442504

48. Sadik CD, Luster AD (2012) Lipid-cytokine-chemokine cascades orchestrate leukocyte recruitment in inflammation. J Leukoc Biol 91: 207–215. doi: 10.1189/jlb.0811402 PMID: 22058421

49. Satpathy SR, Jala VR, Bodduluri SR, Krishnan E, Hegde B, et al. (2015) Crystalline silica-induced leukotriene B_4-dependent inflammation promotes lung tumour growth. Nat Commun 6: 7064. doi: 10.1038/ncomms8064 PMID: 25923988

50. Mahadeo DC, Janka-Junttila M, Smoot RL, Roselova P, Parent CA (2007) A chemoattractant-mediated Gi-coupled pathway activates adenylyl cyclase in human neutrophils. Mol Biol Cell 18: 512–522. PMID: 17135293

51. Liu L, Das S, Losert W, Parent CA (2010) mTORC2 regulates neutrophil chemotaxis in a cAMP- and RhoA-dependent fashion. Dev Cell 19: 845–857. doi: 10.1016/j.devcel.2010.11.004 PMID: 21145500

52. Tauro BJ, Greening DW, Mathias RA, Ji H, Mathivanan S, et al. (2012) Comparison of ultracentrifugation, density gradient separation, and immunoaffinity capture methods for isolating human colon cancer cell line LIM1863-derived exosomes. Methods 56: 293–304. doi: 10.1016/j.ymeth.2012.01.002 PMID: 22285593

53. Comer FI, Parent CA (2006) Phosphoinositide 3-kinase activity controls the chemoattractant-mediated activation and adaptation of adenylyl cyclase. Mol Biol Cell 17: 357–366. PMID: 16267269

54. McCann CP, Kriebel PW, Parent CA, Losert W (2010) Cell speed, persistence and information transmission during signal relay and collective migration. J Cell Sci 123: 1724–1731. doi: 10.1242/jcs.060137 PMID: 20427323

55. McColl SR, Betts WH, Murphy GA, Cleland LG (1986) Determination of 5-lipoxygenase activity in human polymorphonuclear leukocytes using high-performance liquid chromatography. J Chromatogr 378: 444–449. PMID: 3016012